FARADAY ROTATION, MAGNETIC FIELDS,

and the

FIFTH PHASE OF THE INTERSTELLAR MEDIUM

(Title slide from MVU III)

Carl Heiles, UC Berkeley

MAGNETIC FIELDS

and the

FIFTH PHASE OF THE INTERSTELLAR MEDIUM

(Assigned Title slide for MVU IV)

Carl Heiles, UC Berkeley

ENHANCED FARADAY ROTATION

and

TURBULENCE

in the

WARM PARTIALLY IONIZED MEDIUM

Carl Heiles, UC Berkeley

FARADAY ROTATION MEASURES…

THEN (Oren & Wolfe 1995)—499 sources

region A. This region is roughly coincident with Loop II of the Galactic radio continuum, which is believed to be due to a shell of gas surrounding a nearby (≈ 100 pc) hot bubble in the interstellar medium (Elliott & Meaburn 1970; Berkhuijsen, Haslam, & Salter 1971; Vallée 1982). Recently Vallée (1993) derived a magnetic field strength of 17 μG in the shell material from the SKB RM data, which is consistent with amplification of the ambient interstellar magnetic field via "snowplow" compression of the medium in which the field is flux-frozen. (4) There are several sources with RMs very different from the RMs of their neighbors (for instance, the large positive RM near the north Galactic pole). These aberrant RMs may be extragalactic in origin, or may be due to small scale galactic features of angular size less than a few degrees. In either case, these RMs do not participate in the correlations noted in (3) and therefore are not useful for determining GRM.

These qualitative observations suggest a method of estimating the GRM for a given line of sight: average the RMs of nearby sources, excluding the aberrant RMs mentioned in (4) above. However, it is still necessary to define what we mean by "nearby" and what we mean by "aberrant." We consider the second of these first.

We wish to exclude RMs which are apparently not drawn from the same RM distribution as their neighbors. We adopt the following prescription, similar to that of Simard-Normandin, & Kronberg (1980): for each source in the SKB catalog we find the average and standard deviation of sources in its neighborhood (we will make our definition of "neighborhood" explicit below). If the source is different from the average by more than three times the standard deviation, we reject it. We then iterate the procedure until no more sources are rejected. In this fashion, we remove 43 sources from the 542 sources in Figure 2. The resulting "cleaned" RM sky map is presented in Figure 3.

We now set out to further quantify the previously mentioned trends using the "cleaned" SKB data. The histograms of the RMs in latitude bins 0°–20°, 20°–40°, 40°–60°, and 60°–90° are plotted in Figure 4. The Gaussian sigmas of fits to these distributions are 99, 44, 21, and 14 rad m^{-2}, respectively. From the distribution in the 60°–90° latitude bin we infer that the typical observed extragalactic RM is no greater than 14 rad m^{-2} in amplitude. Thus the GRM is the dominant component of the observed RM for most sources with $|b| \leq 40°$. The GM below $|b| = 20°$ are so large that sources at such latitudes are useless for RRM studies. For this reason we have included only sources with $|b| > 20°$ in our survey.

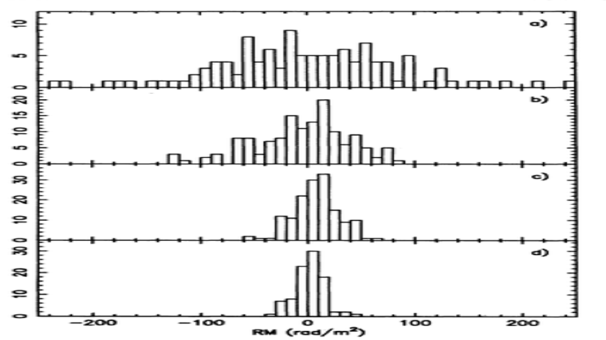

FIG. 4.—Histograms of the RMs of the "cleaned" SKB catalog in latitude bins: (*a*) $0° \leq |b| < 20°$, (*b*) $20° \leq |b| < 40°$, (*c*) $40° \leq |b| < 60°$, and (*d*) $60° \leq |b| \leq 90°$. The RMs for 0807−38 (RM = 272, $b = -3.2$), 2037+51 (−258, 6.0), 2106+49 (−359, 1.3), and 2243+39 (−275, −17.1) are not shown. Note that all of these large RMs are in the lowest latitude bin.

Let us now consider what is meant by "nearby." When determining the GRM for a position, it is desirable to include as many RMs as possible in order to obtain a robust average. The mean density of sources in the "cleaned" SKB sample is only one source per 83 deg^2. Therefore, to obtain a sample of several sources to average, one must consider a region around the position of interest which is tens of degrees on a side. From visual inspection, it appears that RMs are correlated over such scales, so a reasonable sample should be obtainable. We refer

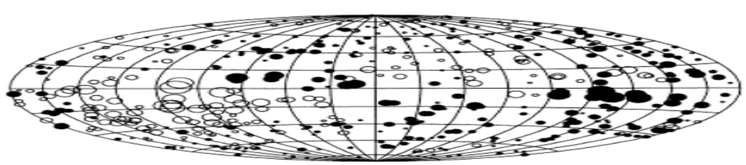

FIG. 3.—RMs of the 499 extragalactic sources of the "cleaned" SKB catalog, presented as in Fig. 2

and NOW (Taylor, Stil, Sumsrum 2009): ‘best guess’ RMs for 37,543 NVSS sources. That’s more than one per square degree! The angular resolution is comparable to the WHAM (Hα) and LAB 21-cm line HI) surveys!

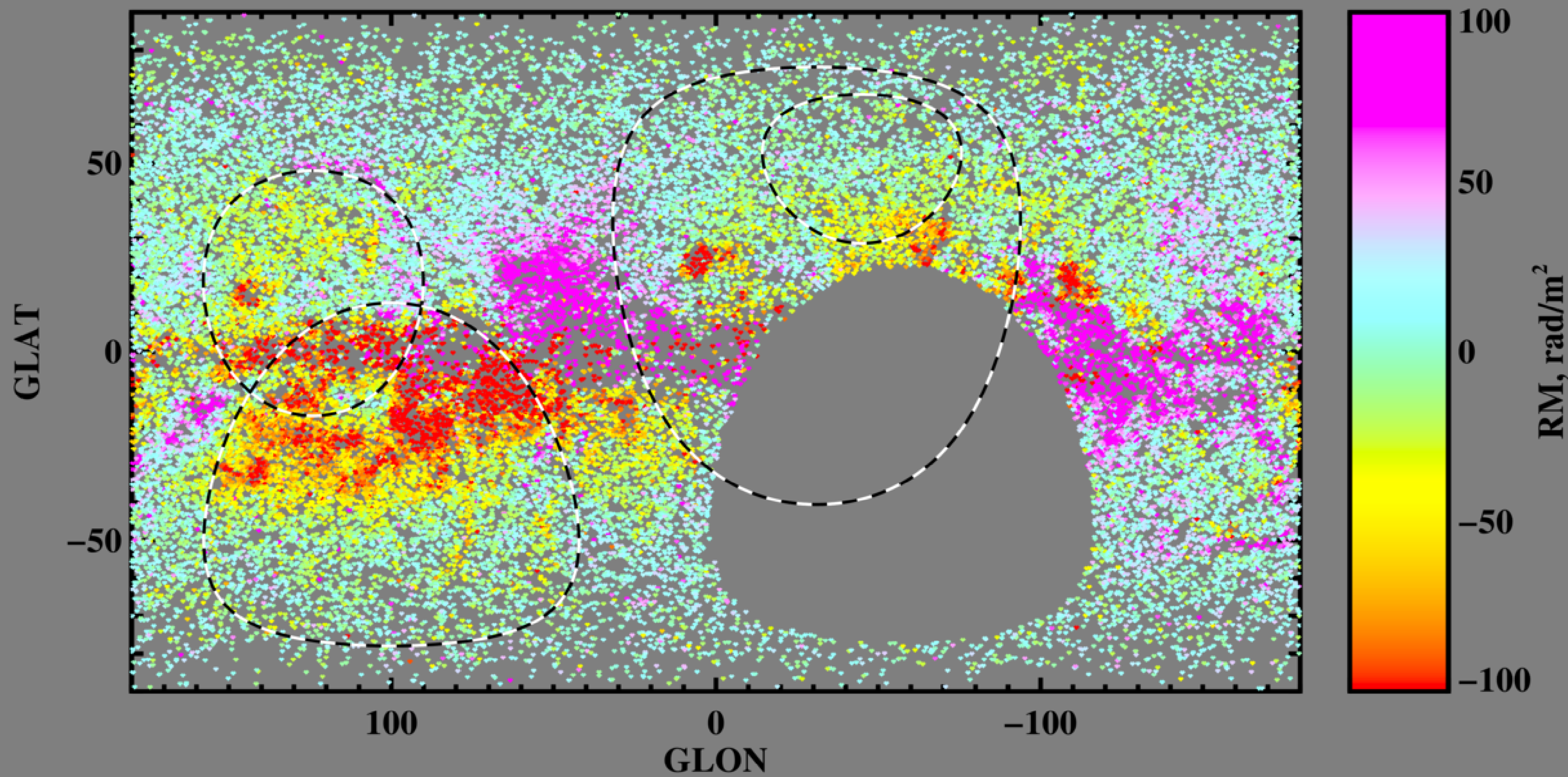

We'll compare the RM, HI, and Hα maps. We'll look at different velocity ranges so that we can isolate individual structures along the line of sight. We'll do detailed comparisons by 'flashing'.

+4 to +14 km/s

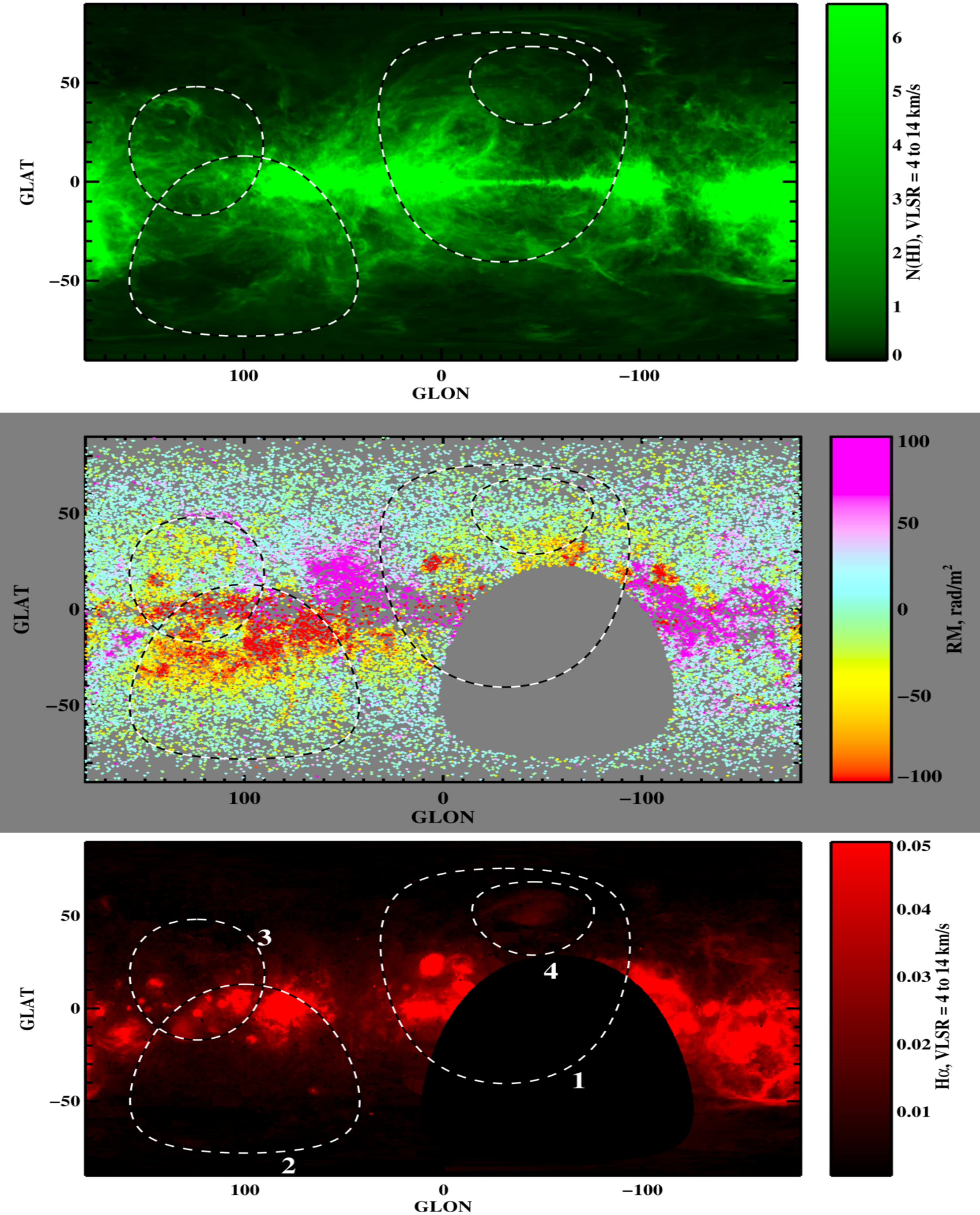

HI: +4 to +14 km/s

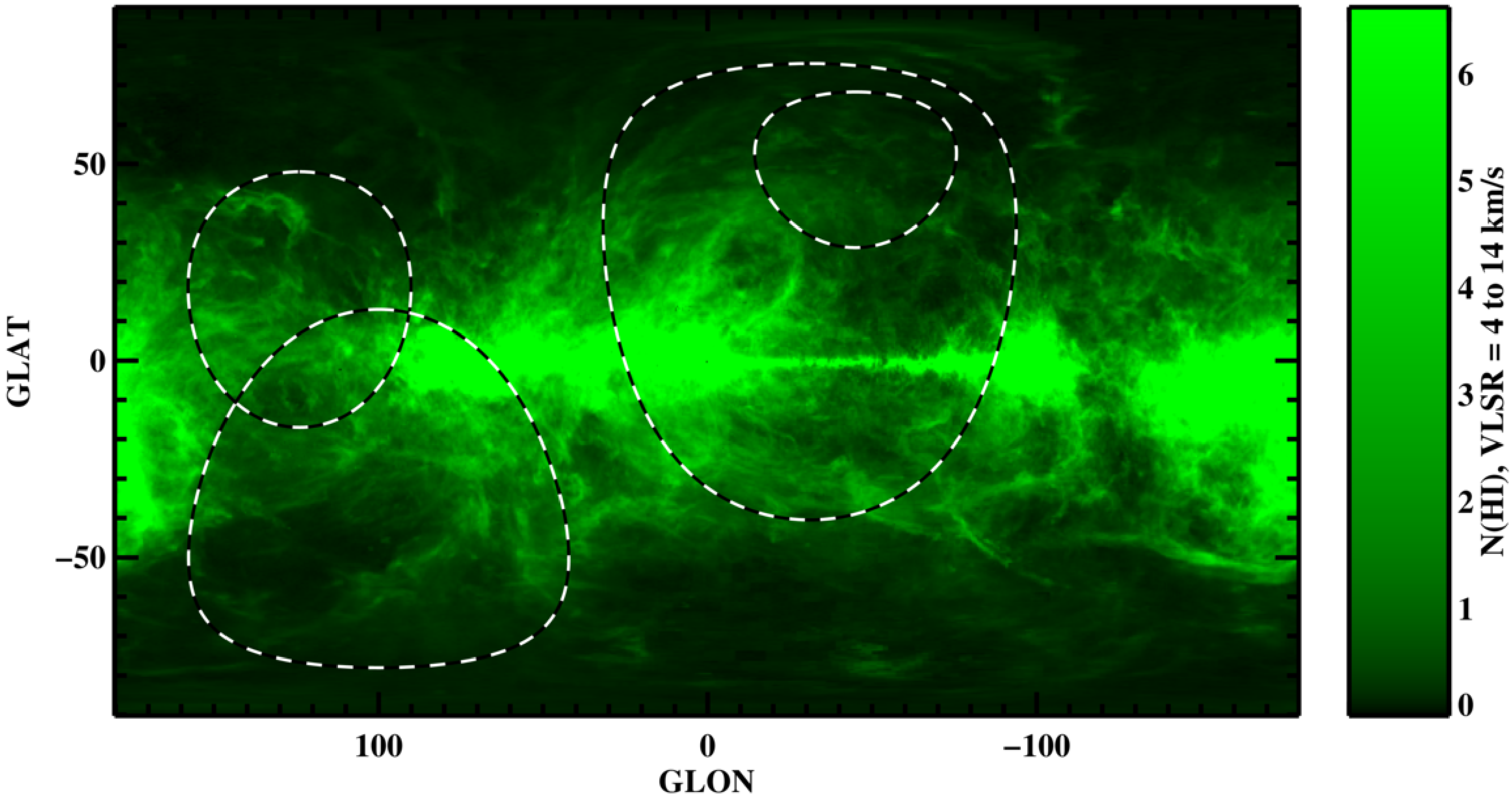

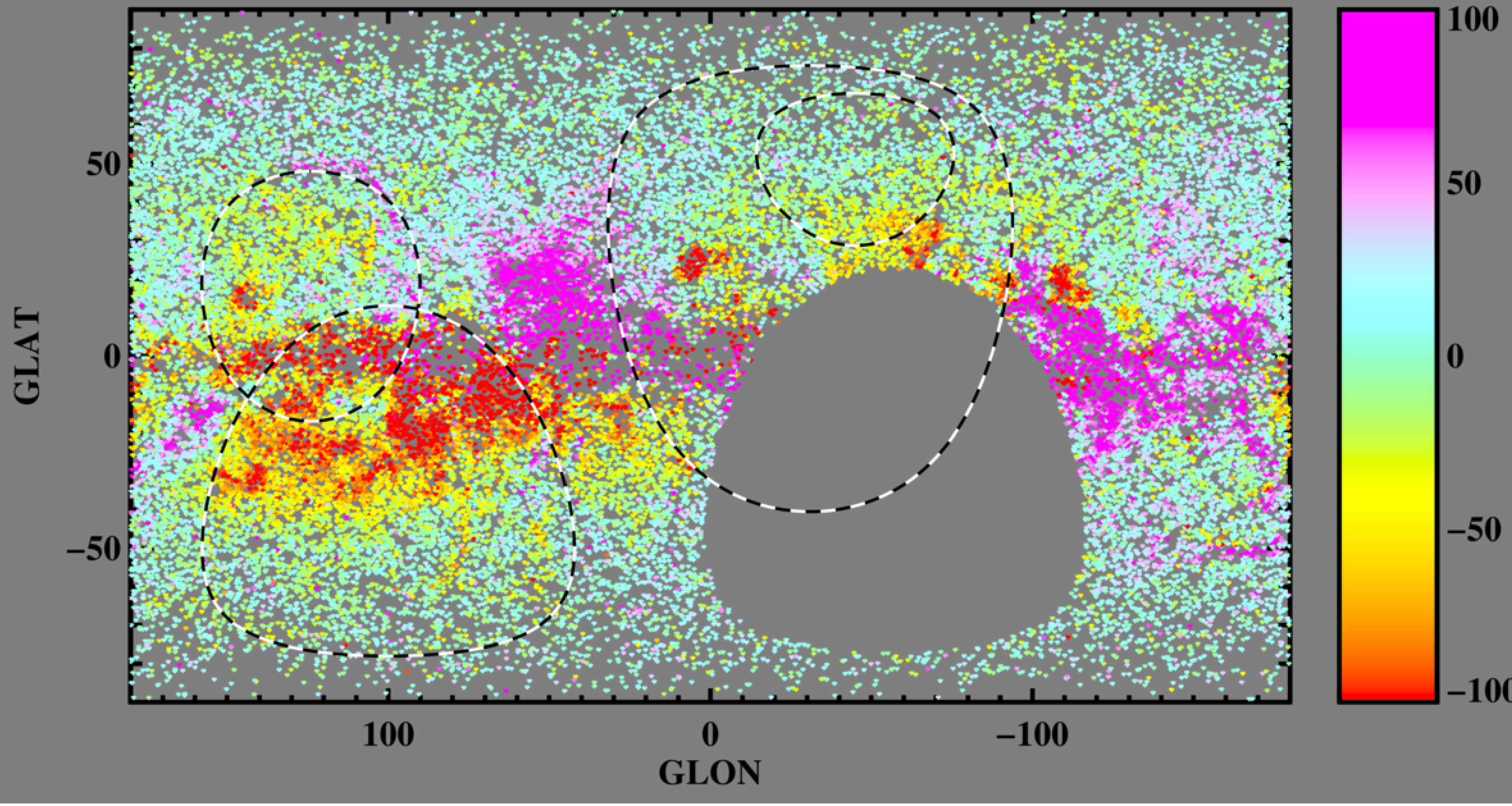

50
0
−50
GLAT
100
0
−100
GLON
100
50
0
−50
−100
RM, rad/m²

Hα: +4 to +14 km/s

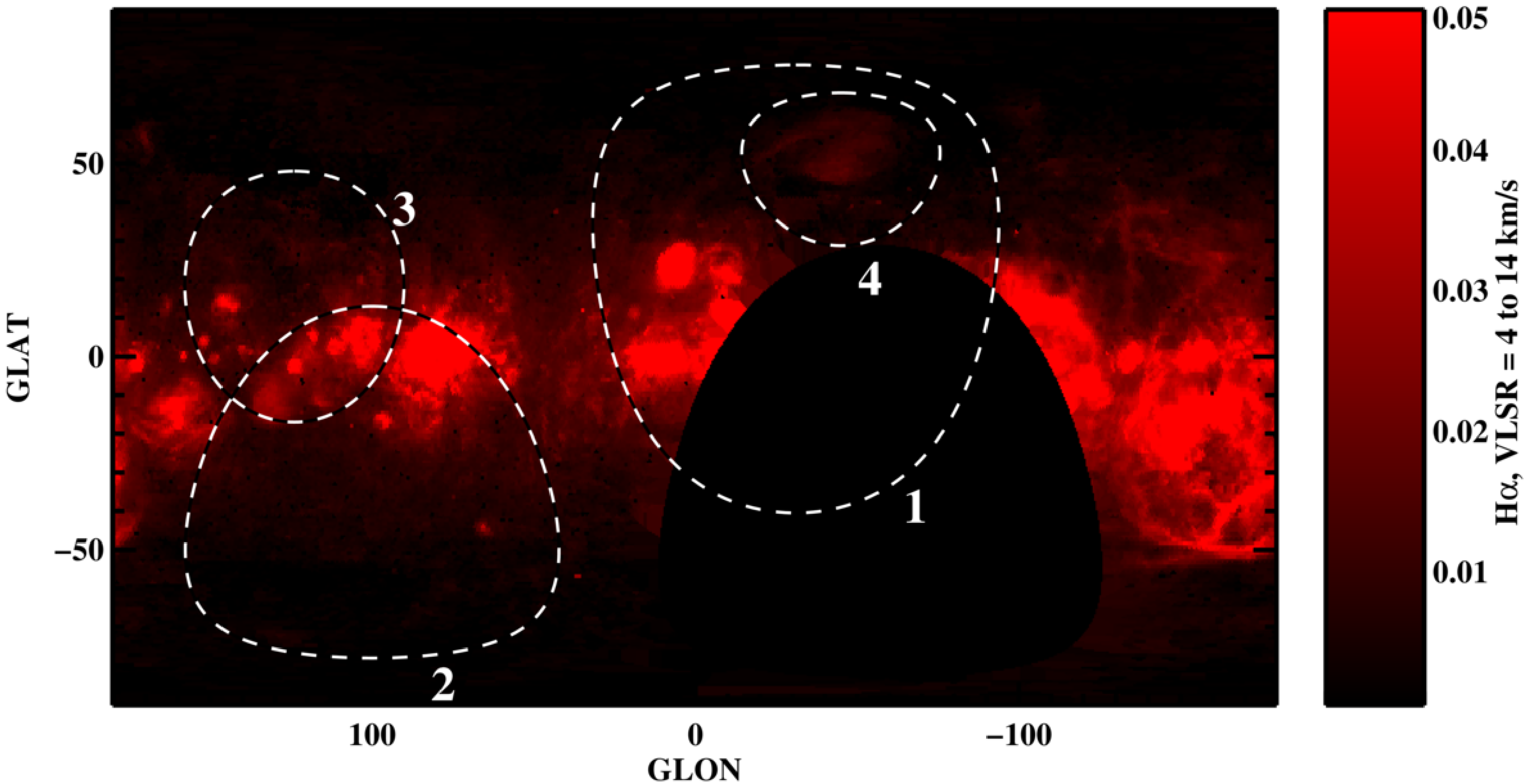

50
0
−50
GLAT
100
0
−100
GLON
1
2
3
4
0.05
0.04
0.03
0.02
0.01
Hα, VLSR = 4 to 14 km/s

-52 to -50 km/s

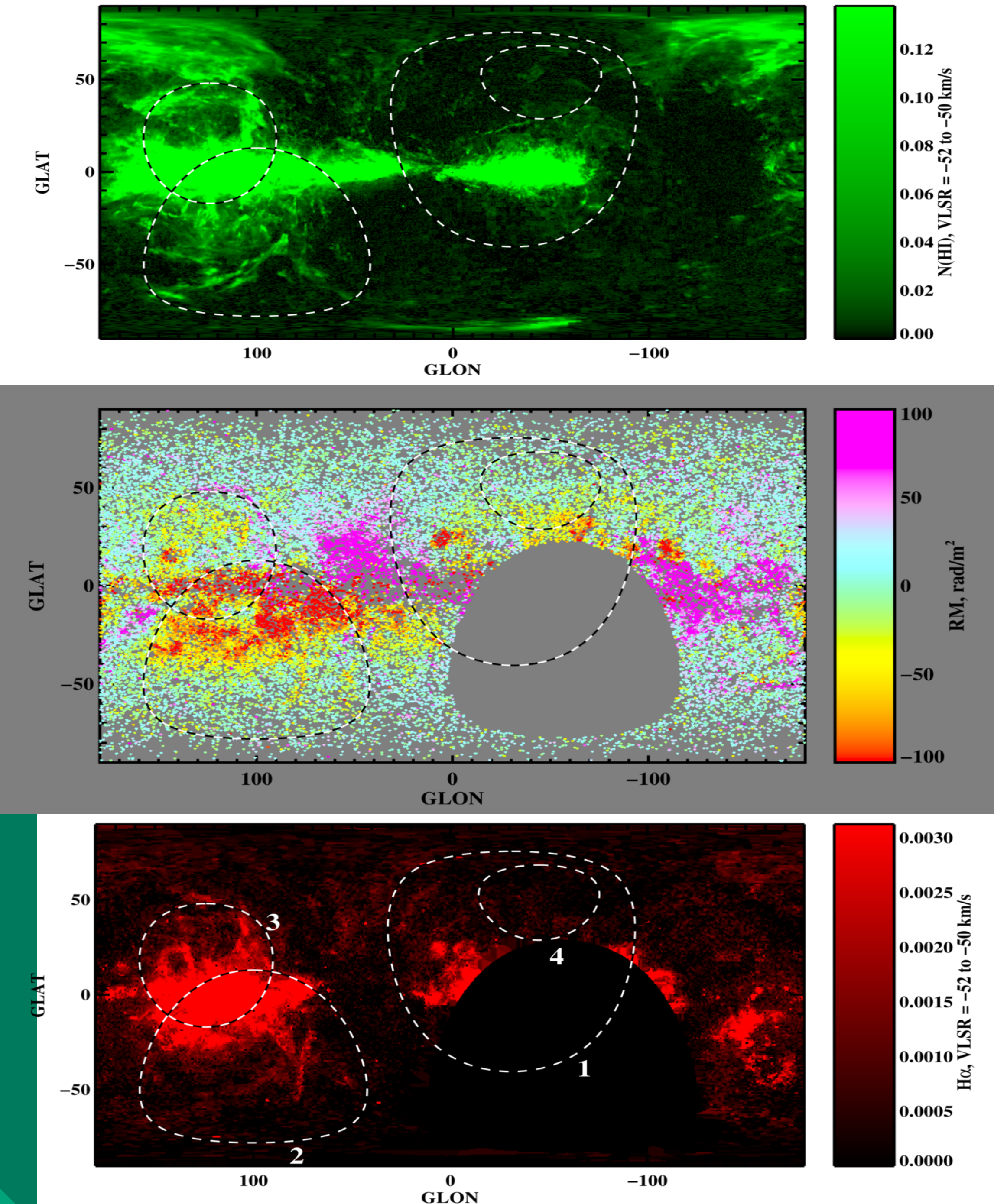

50
0
−50
GLAT
100
0
−100
GLON
0.12
0.10
0.08
0.06
0.04
0.02
0.00
N(HI), VLSR = −52 to −50 km/s
50
0
−50
GLAT
100
0
−100
GLON
100
50
0
−50
−100
RM, rad/m²
50
0
−50
GLAT
3
4
1
2
100
0
−100
GLON
0.0030
0.0025
0.0020
0.0015
0.0010
0.0005
0.0000
Hα, VLSR = −52 to −50 km/s

HI: -52 to -50 km/s

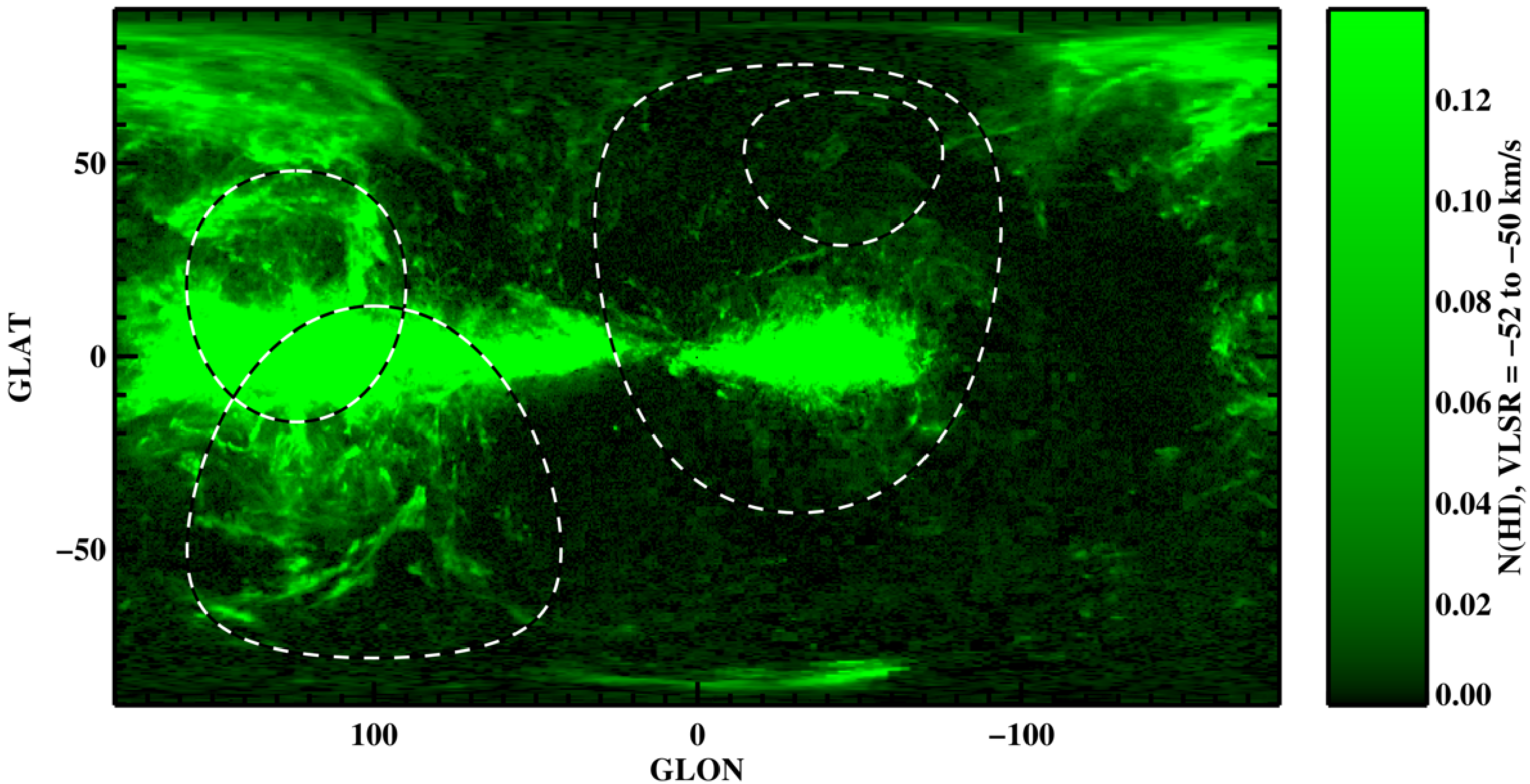

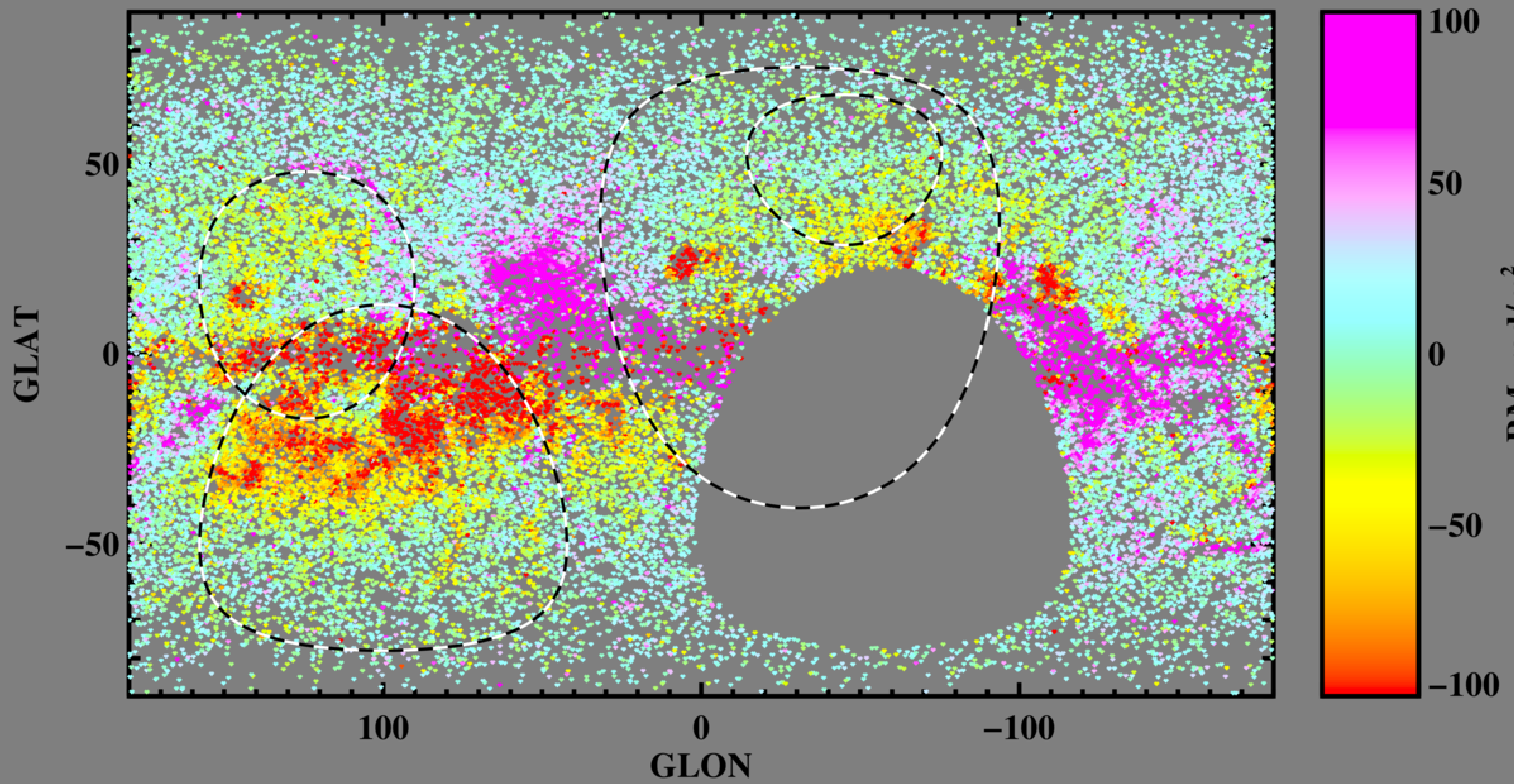

50
0
−50
GLAT
100
0
−100
GLON
100
50
0
−50
−100
RM, rad/m2

Hα: -52 to -50 km/s

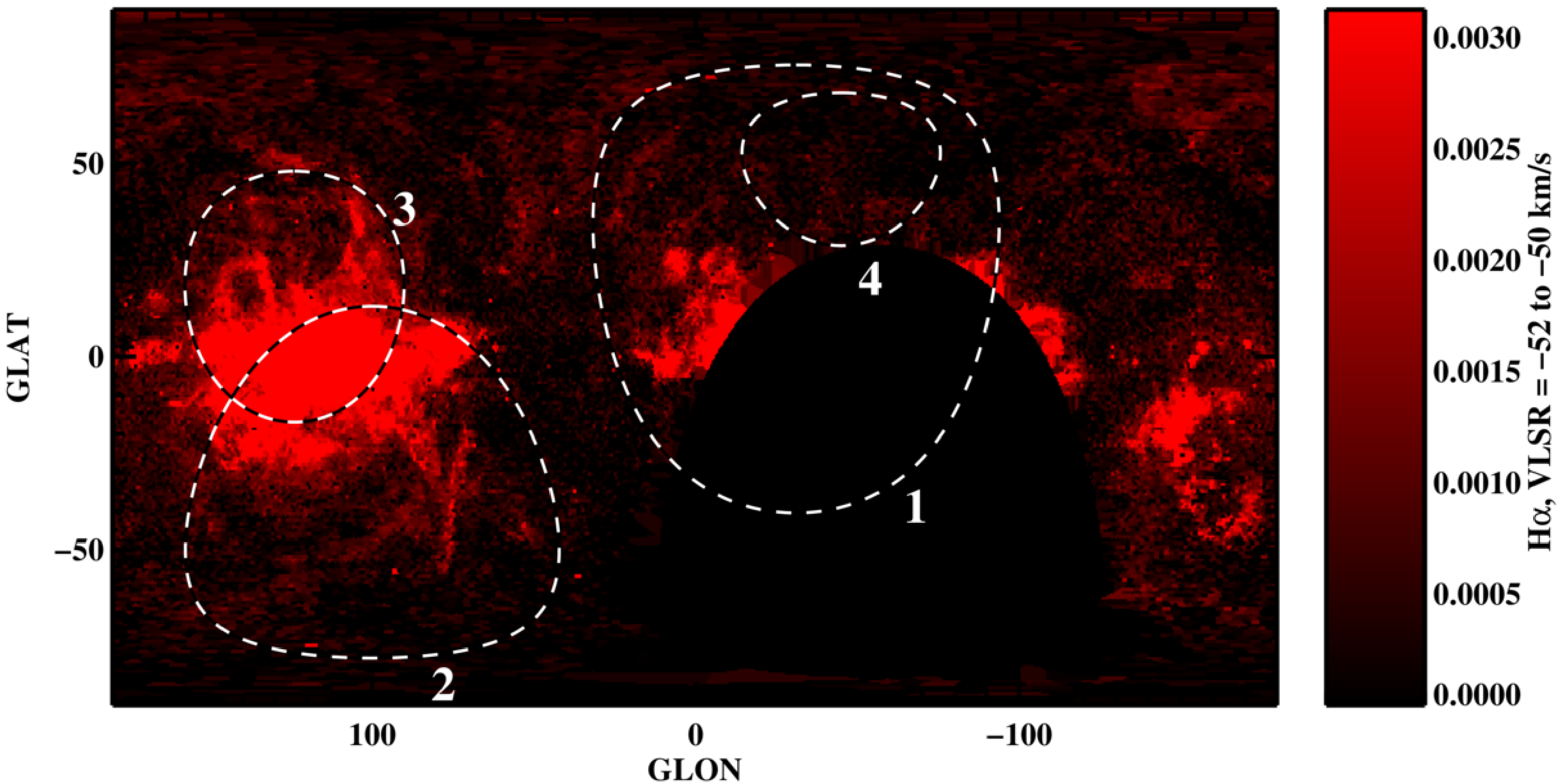

-21 to -19 km/s

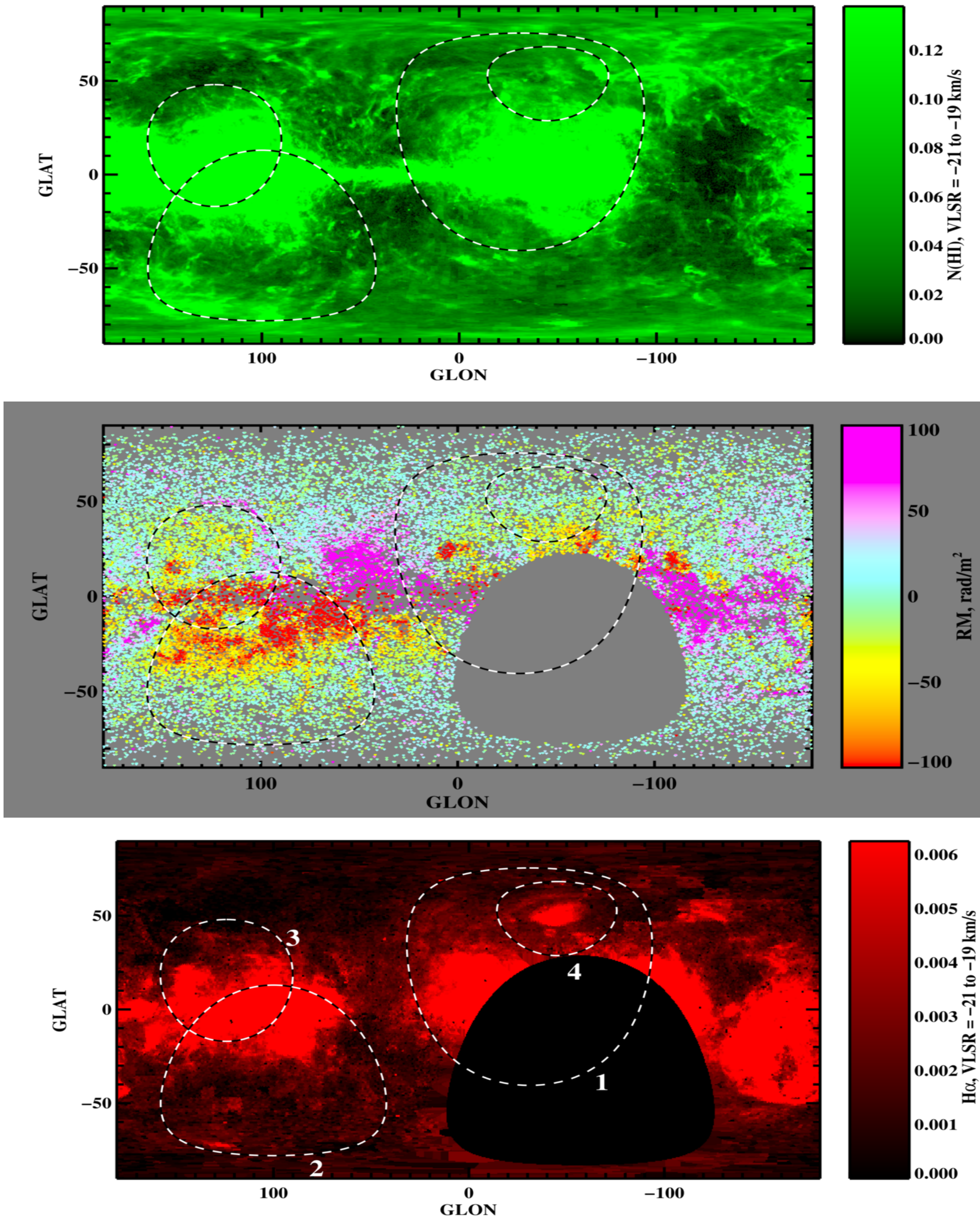

GLAT
GLON
N(HI), VLSR = −21 to −19 km/s
RM, rad/m^2
Hα, VLSR = −21 to −19 km/s
1
2
3
4

HI: -21 to -19 km/s

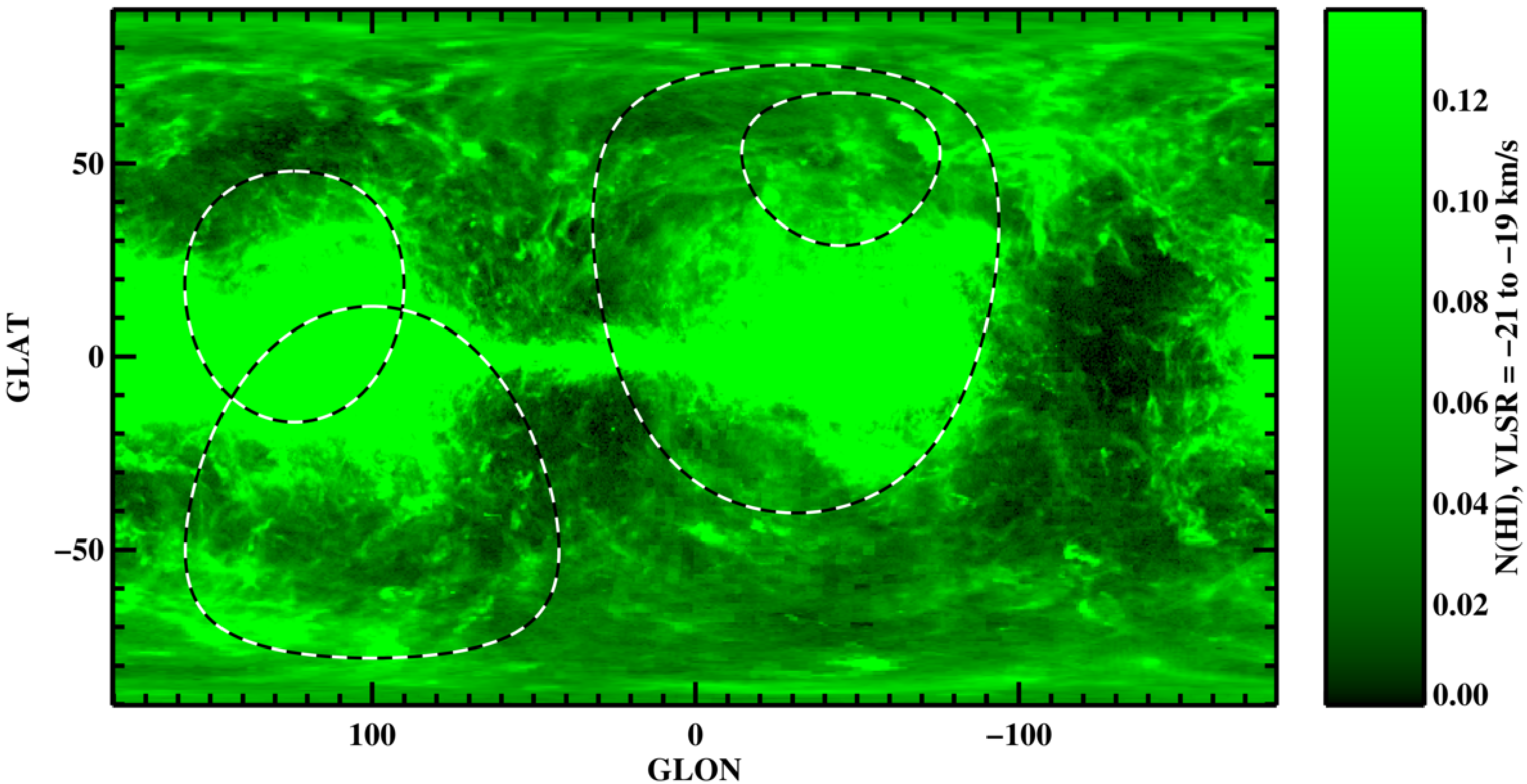

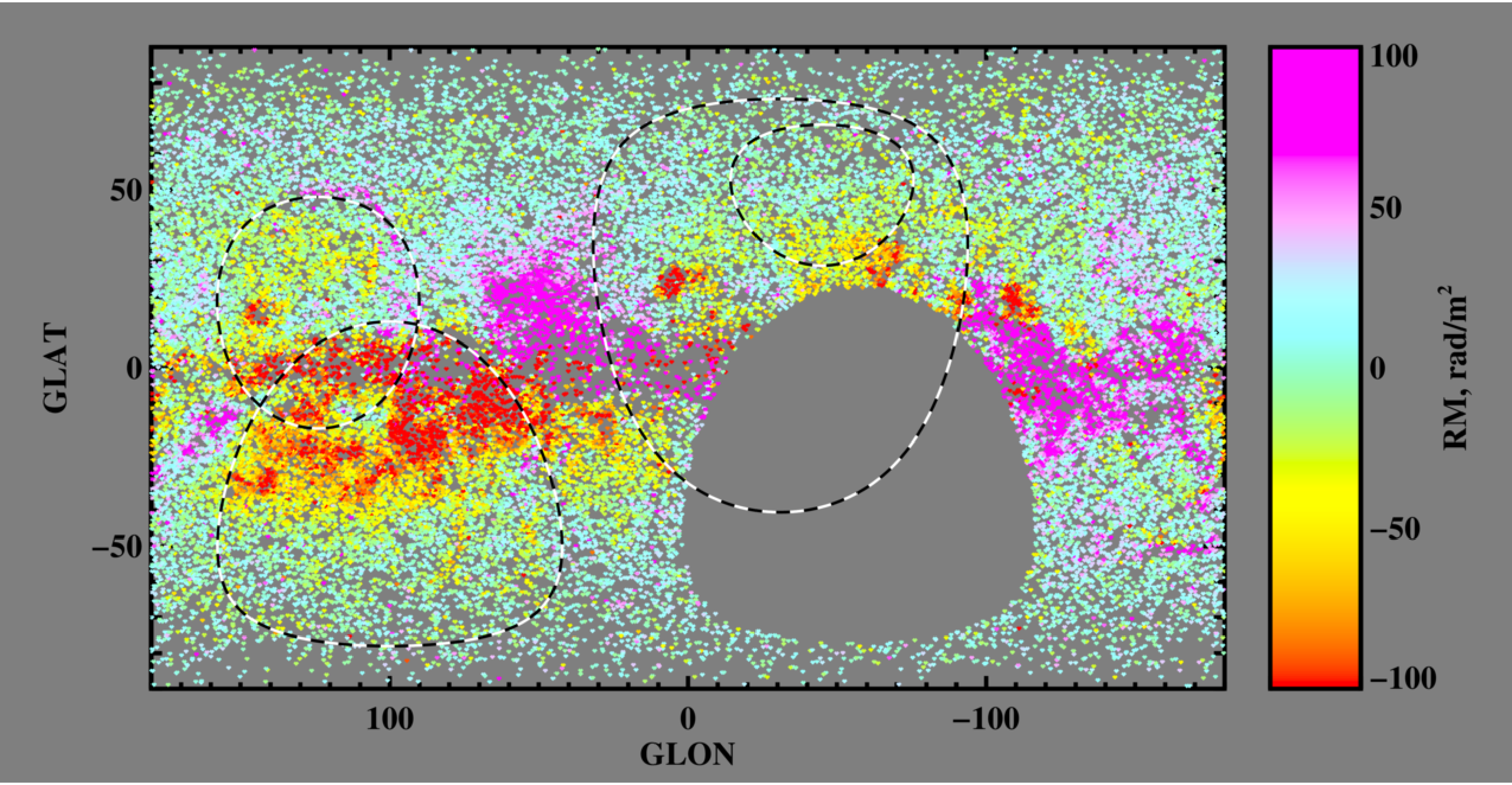
GLAT
GLON
RM, rad/m^2
100
50
0
−50
−100
100
0
−100
100
50
0
−50
−100

Hα: -21 to -19 km/s

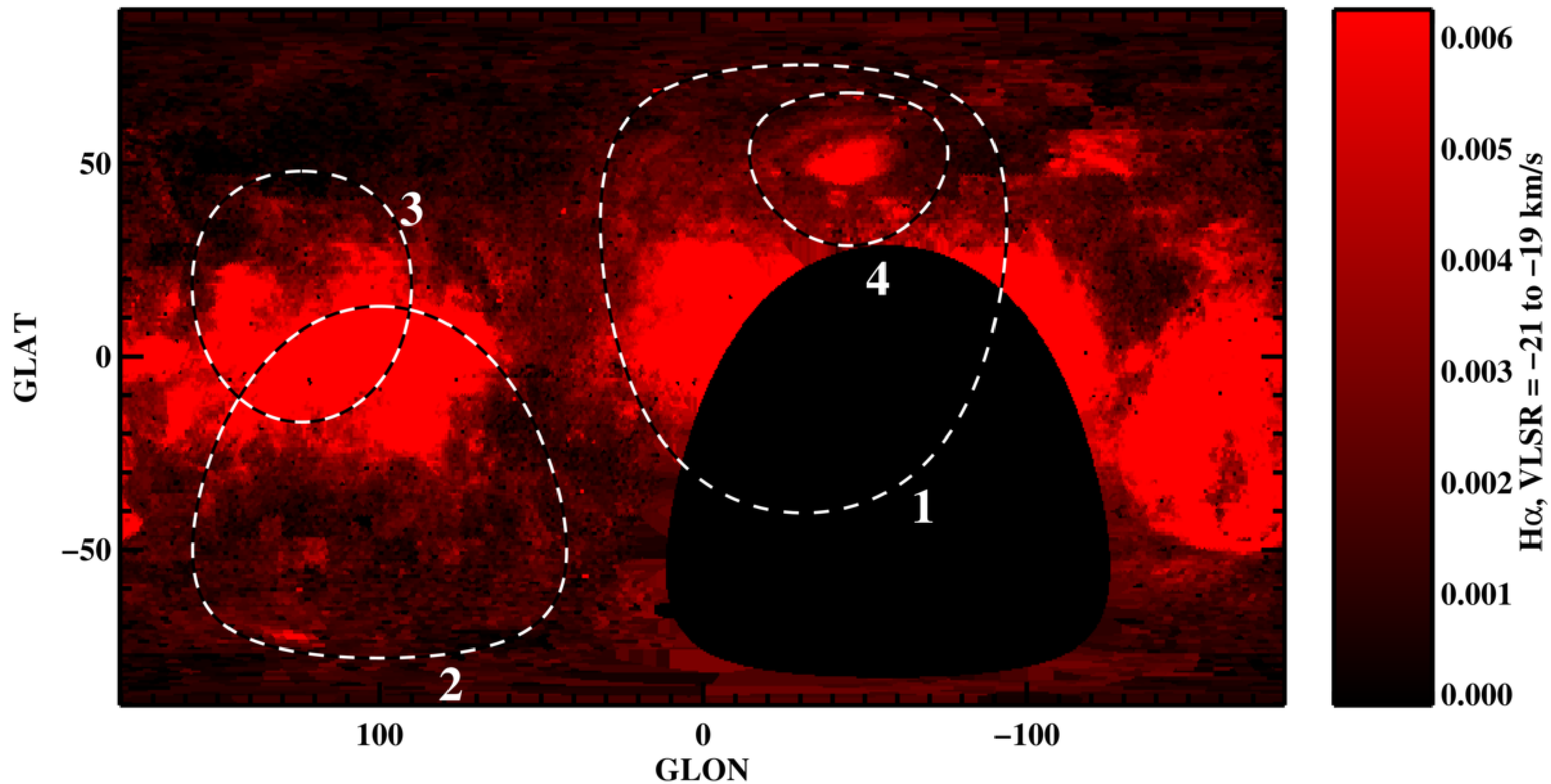

What we saw in the first two:

--RM structures lie near morphologically similar HI and Hα structures.

--HOWEVER, the RM structures seem OFFSET IN POSITION: they don't lie on top of either the HI or Hα.

--Many HI and Hα structures are morphologically similar, but are also OFFSET IN POSITION.

WHAT'S GOING ON?

The Story has several aspects. An important one is:

The Warm Partially Ionized Medium

Current View: The Four Phases…and the *FIFTH*

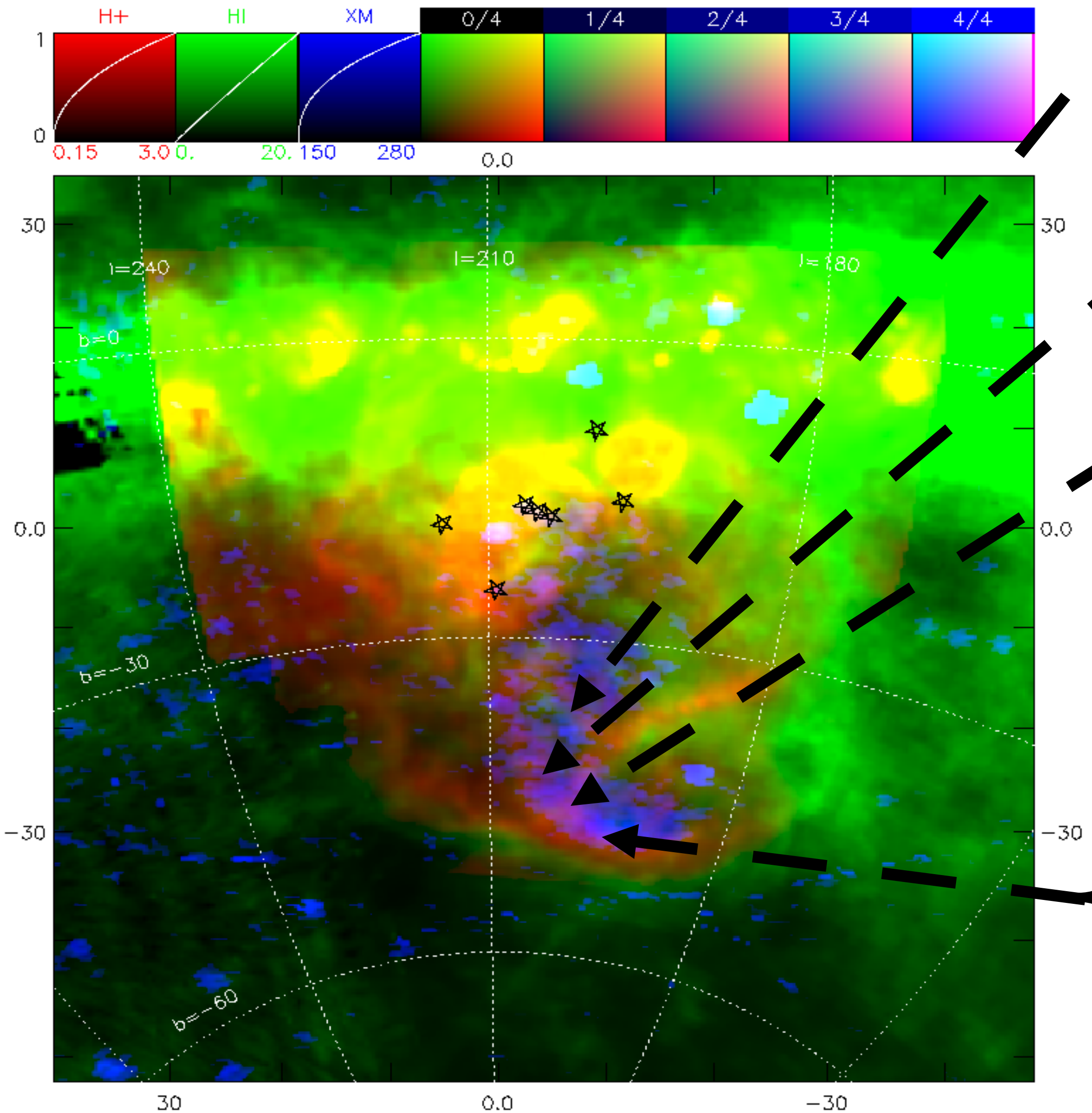

HIM:
T ~ 2 x 106 K
xe = 1; Collisional

WIM:
T ~ 0.8 x 104 K
xe = 1; Stellar UV

WPIM:
T ~ 0.5 x 104 K
xe ~ 0.1 – 0.9;
Soft XR (from HIM),
Stellar UV

WNM:
T ~ 0.5 x 104 K
xe ~ 10-2; Cosmic Rays

CNM:
T ~ 50 K
xe ~ 10-4; Carbon+

The WIM is starlight photoionized, xe~1.0, like HII regions. Starlight comes from the Orion association; the photons travel unimpeded through the HIM in the superbubble interior. High Emission Measure (EM =[ne Ne]), hence high H-alpha (WHAM) visibility.

Traveling outwards, the starlight photons get used up producing the WIM. Then the X-Ray photons from the interior HIM take over, producing The WPIM with smaller ionization fraction, probably xe~0.5 +/- 0.45. When they're used up, we have the CNM.

The ``Local Interstellar Clouds'' (LIC – Redfield & Linsky) are WPIM, with xe~0.5.

(M/O 1977)

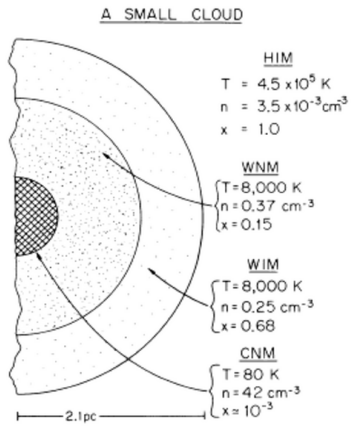

Fig. 1

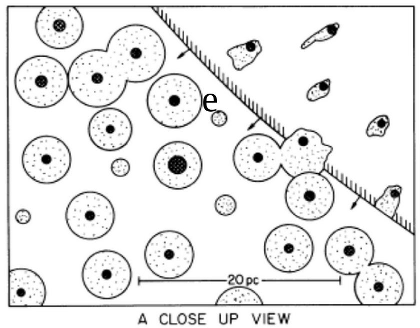

Fig. 2

Fig. 1.—Cross section of a characteristic small cloud. The crosshatched region shows the cold core, which gives the usual optical absorption lines. Next is the warm neutral medium (WNM) with ionization produced by soft X-ray background. The outer layer (WIM) is gas largely ionized by stellar UV background. Typical values of hydrogen density n, temperature T, and ionization $x = n_e/n$ are shown for each component, except that a higher than average value of the soft X-ray flux has been assumed in order to produce a significant amount of WNM at this pressure.

Fig. 2.—Small-scale structure of the interstellar medium. A cross section of a representative region 30 pc × 40 pc in extent is shown, with the area of the features being approximately proportional to their filling factors. A supernova blast wave is expanding into the region from the upper right. The radius of the neutral cores of the clouds (represented by crosshatching) ranges from about 0.4 to 1 pc in this small region; all the clouds with cores have warm envelopes (*dotted regions*) of radius $a_w \sim 2.1$ pc. A few clouds are too small to have cores. The envelopes of clouds inside the SNR are compressed and distorted.

compensate for it in the previous work in this paper by simply decreasing the assumed supernova energy E_{51} by ~30%, a change which would have negligible effect on any of the calculated quantities.

b) Warm Neutral Medium

We estimate from Chevalier's (1974) calculations that soft X-ray photons in the energy range 40–120 eV ($h\bar{\nu}$ = 60 eV) are produced in amount $\epsilon_x = 1.1 \times 10^{-16} S_{-13} E_{51}$ photons cm^{-3} s^{-1}. These will penetrate through the

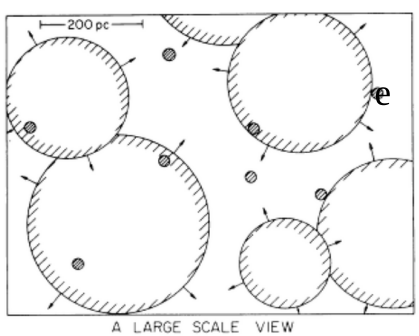

Fig. 3.—Large-scale structure of the interstellar medium. The scale here is 20 times greater than in Fig. 1: the region is 600 × 800 pc. Only SNRs with $R < R_c = 180$ pc and clouds with $a_0 > 7$ pc are shown. Altogether about 9000 clouds, most with $a_w \sim$ 2.1 pc, would occur in a region this size.

IONIZATION AGENT:

Collisional

Cosmic Rays, Soft X-rays

PARTIALLY ionized!

Soft X-rays, Cosmic Rays

Cosmic Rays, C+

Let’s zoom in on the Radio Loop 3 vicinity…

RMs HI

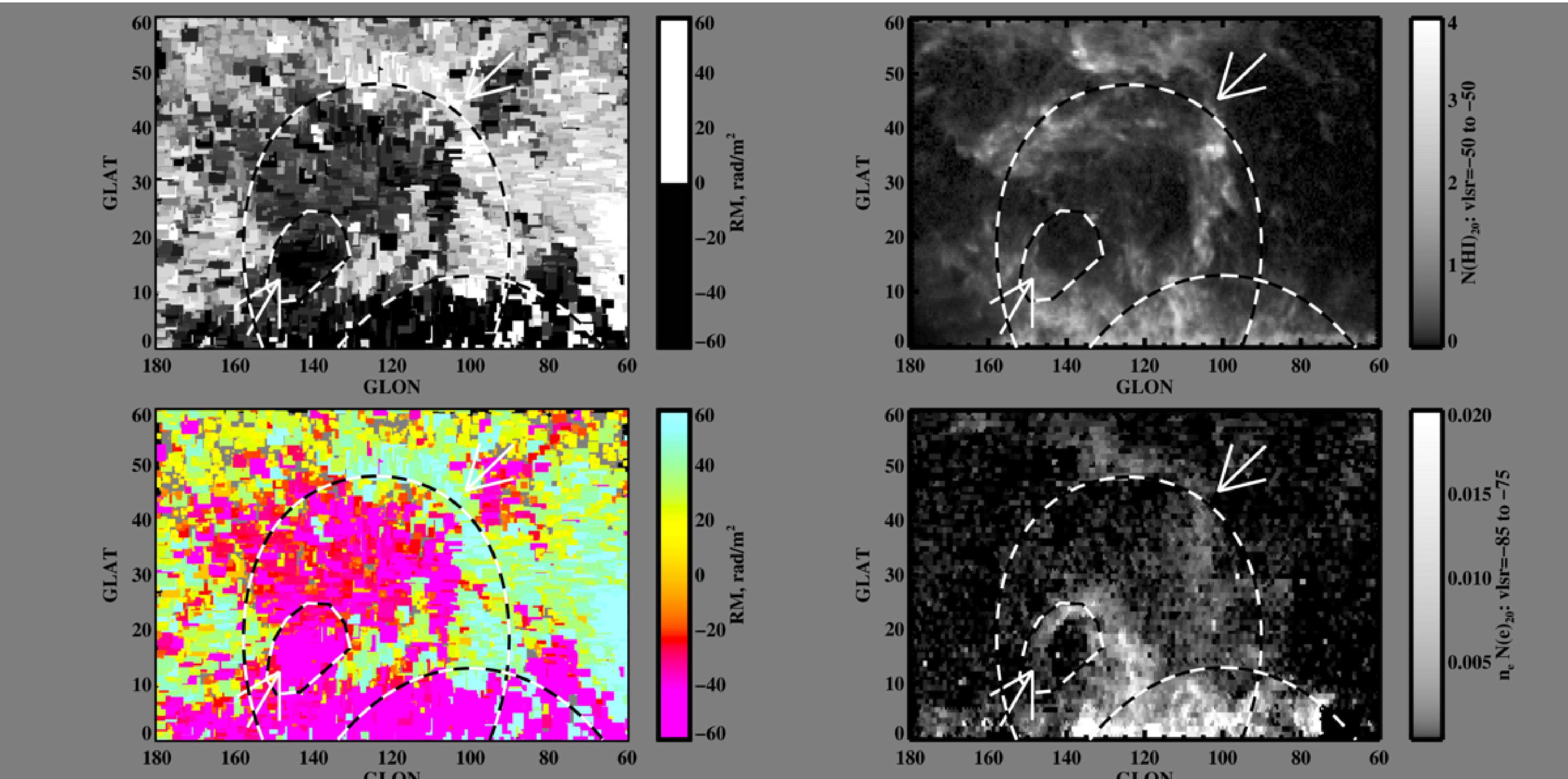

RMs H+

HI

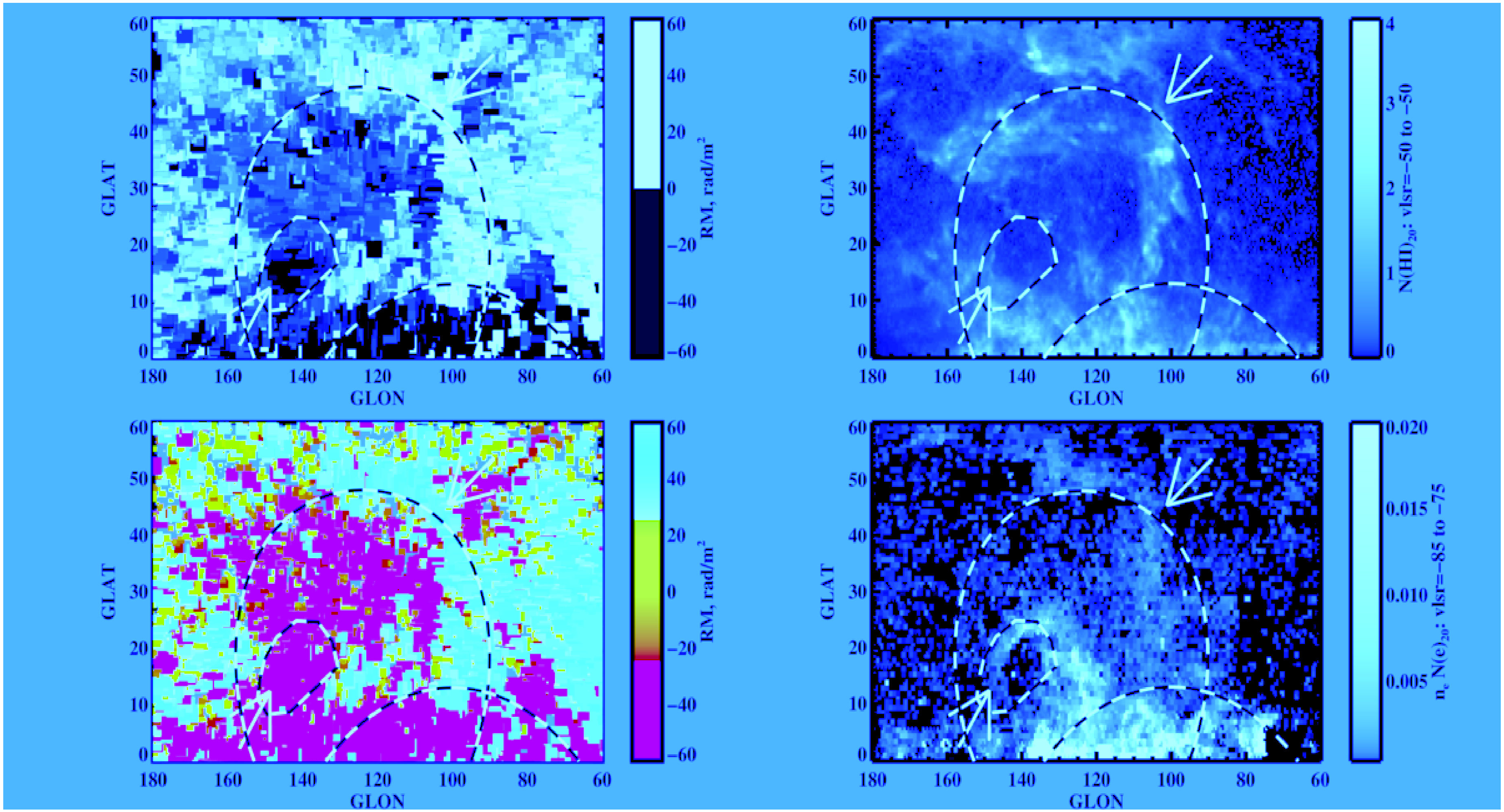

GLAT
GLON
RM, rad/m^2
N(HI)$_{20}$: vlsr=−50 to −50
GLAT
GLON
RM, rad/m^2
n$_e$ N(e)$_{20}$: vlsr=−85 to −75

HI

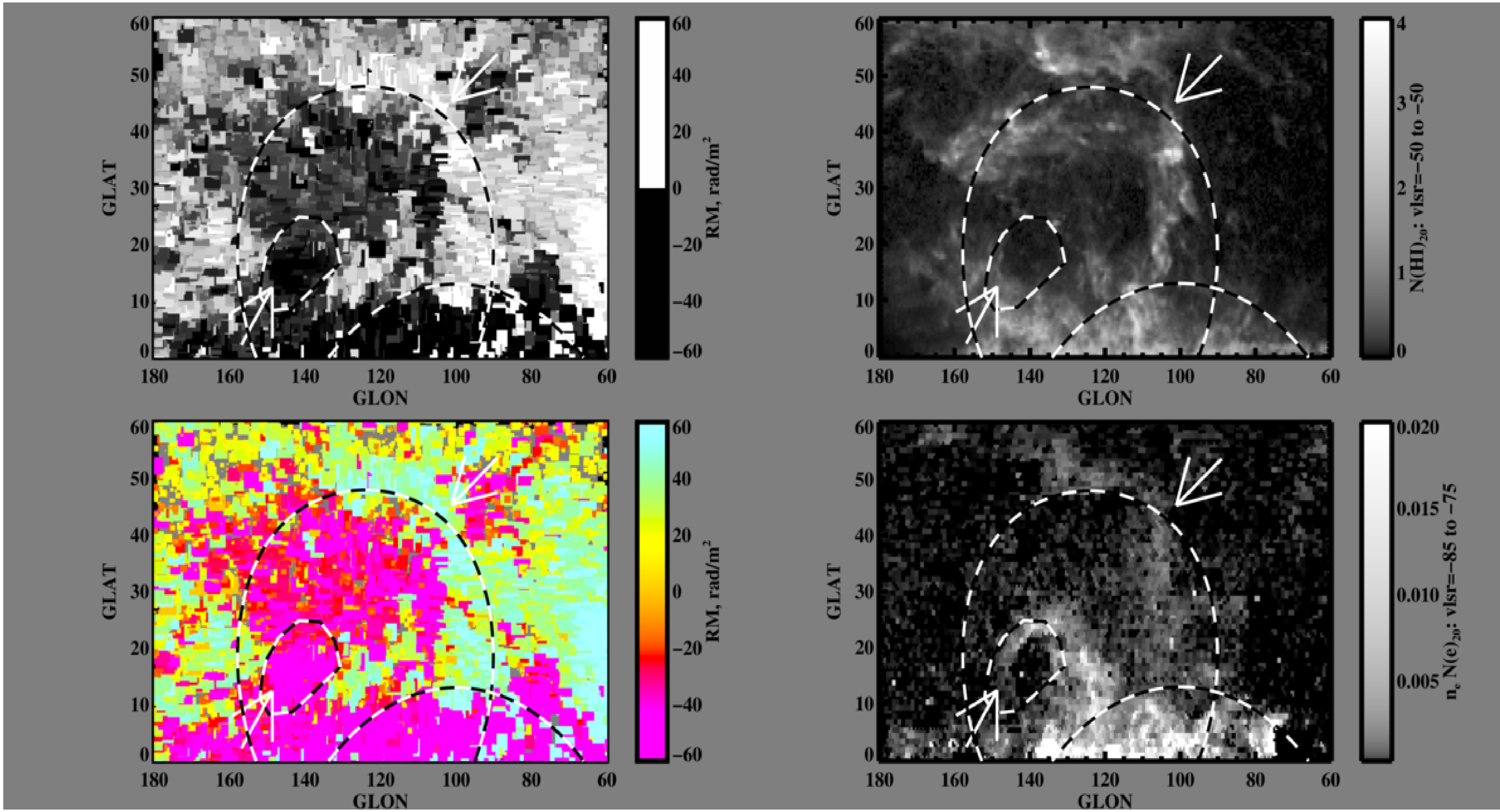
GLAT
GLON
RM, rad/m^2
$N(HI)_{20}$; vlsr=−50 to −50
$n_c N(e)_{20}$; vlsr=−85 to −75

H+

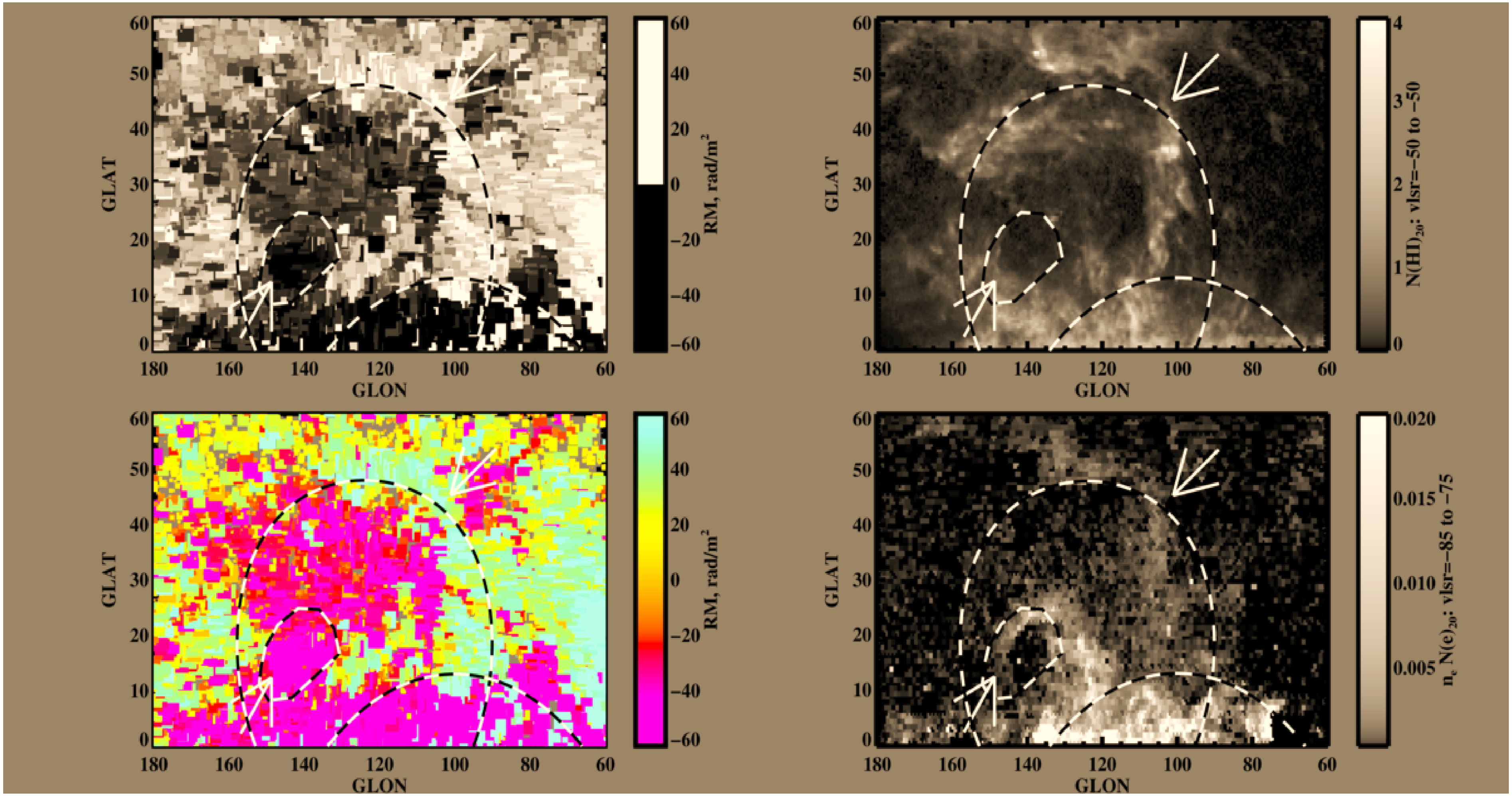

H+

Let's do some numbers…

RM = 0.81 n(e) B|| L rad m-2

EM = n(e) N(e) L cm-6 pc

so [RM/EM] = 0.81 [B|| / n(e)] .

We see ΔRM ~ 100 rad m-2

ΔEM ~ 2.0 cm-6 pc

We can combine these and make a model:

<u>Assumed Distance= 200 pc</u>

n(e) = 0.10 cm-3

2n(e)T=1650 cm-3K

B=7.6 μG

P=16400 cm-3K

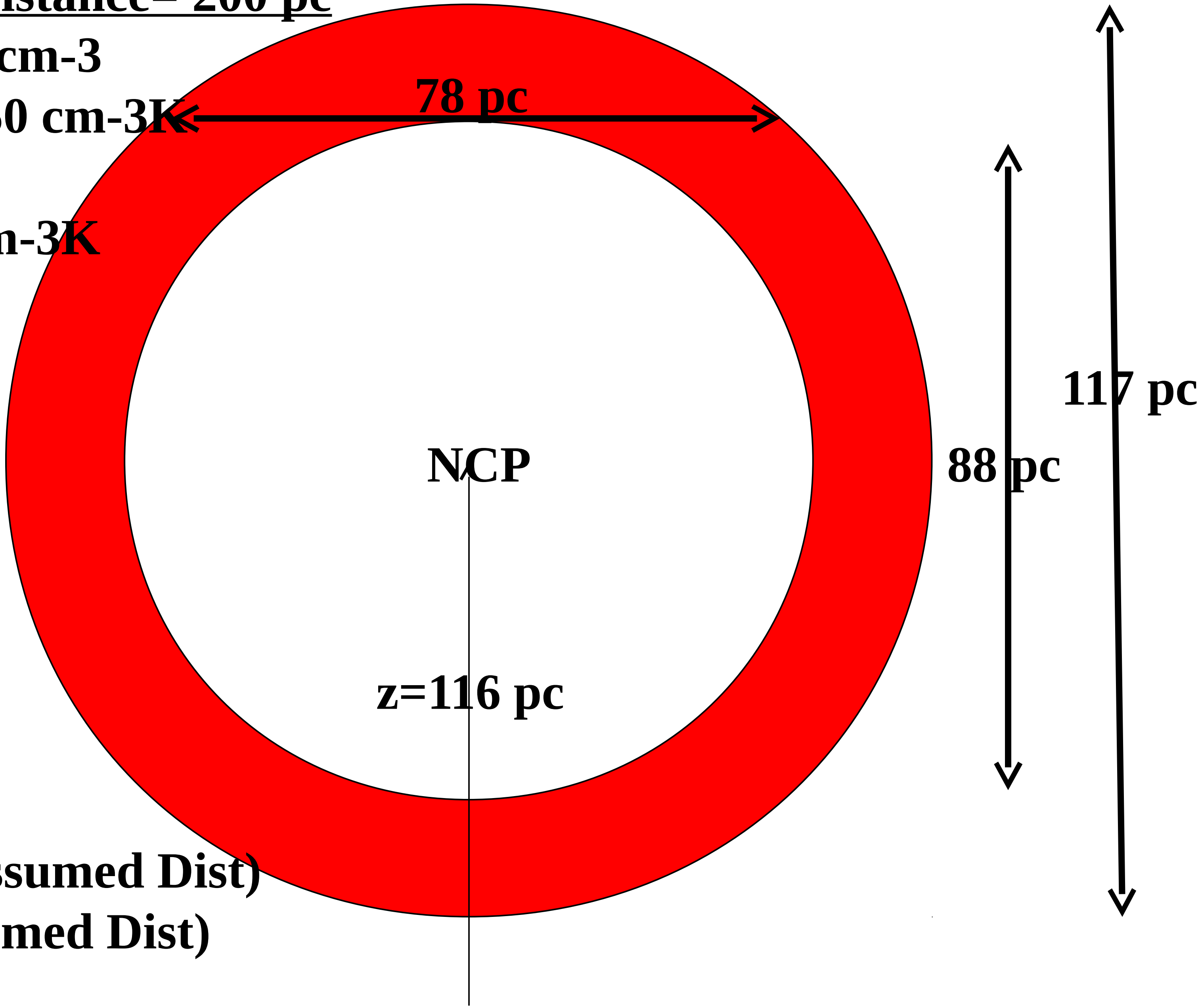

n(e) ~ (1/Assumed Dist)

B ~ (1/Assumed Dist)

Before going ahead, let's consider a puzzle:

$$EM \sim \int n(e)\, n(e)\, dl = N(e)\, n(e)$$
$$RM \sim \int n(e)\, B_{||}\, dl = N(e)\, B_{||}$$

With flux freezing, and perpendicular shocks, we have

$$B \sim n(e)$$

(and, with parallel shocks, B is independent of n(e)). So, for a given column N(e), as n(e) increases we should have

$$\Delta(RM) \sim \Delta(EM) \quad \text{for perpendicular shocks, or}$$
$$\Delta(RM) \sim 0 \text{ for parallel shocks}$$

So how can Δ(RM) ever be bigger than Δ(EM)?

The Answer must lie in:

$$EM \sim \int n(e)\, n(e)\, dl = N(e)\, n(e)$$

$$RM \sim \int n(e)\, B_{||}\, dl = N(e)\, B_{||}$$

i.e., in the DIRECTION of B||, Nothing illustrates this better than the

Orion/Eridanus Superbubble.

Current View: The Four Phases…and the *FIFTH*

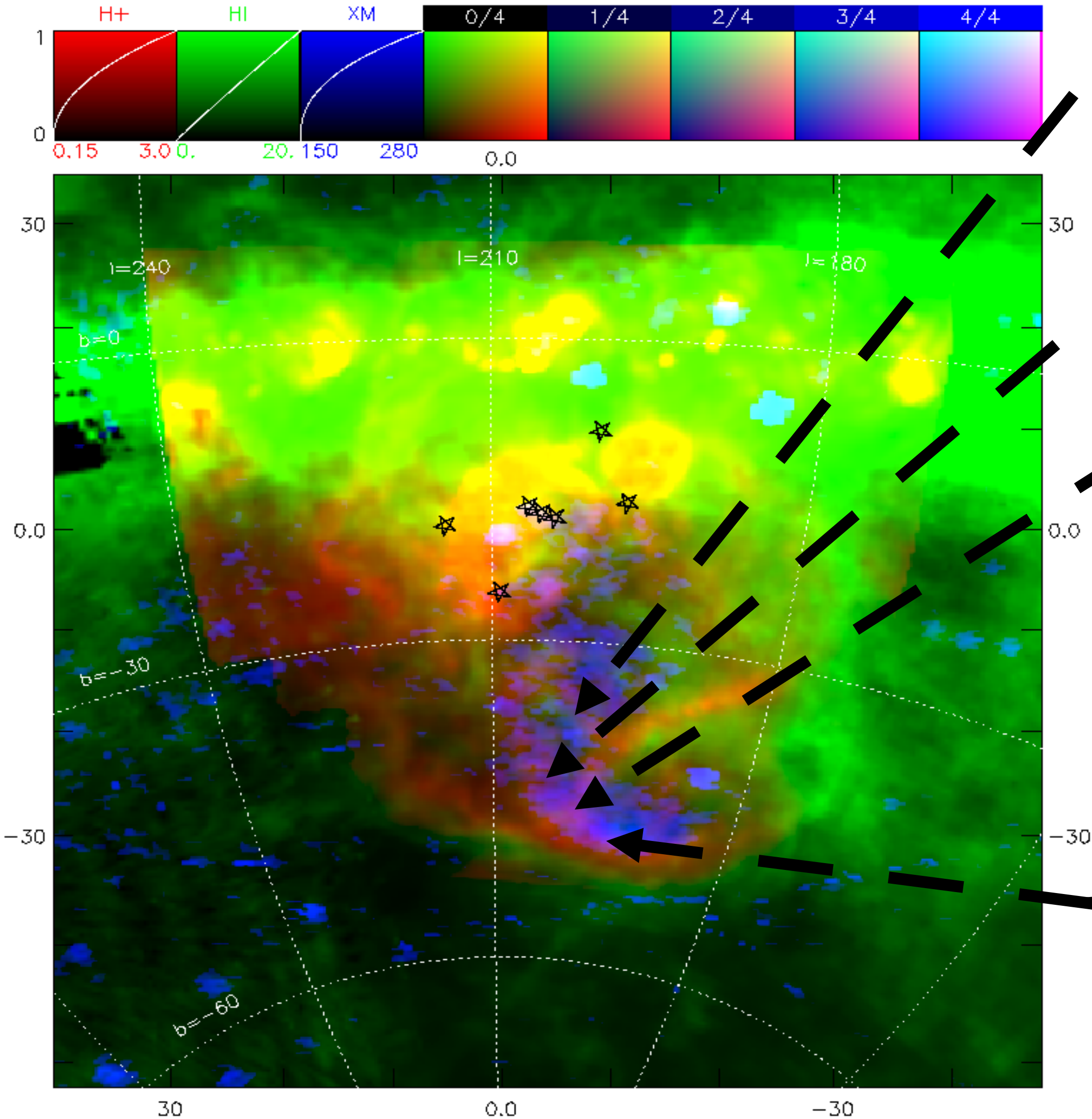

HIM:
T ~ 2 x 106 K
xe = 1; Collisional

WIM:
T ~ 0.8 x 104 K
xe = 1; Stellar UV

WPIM:
T ~ 0.5 x 104 K
xe ~ 0.1 – 0.9;
Soft XR (from HIM),
Stellar UV

WNM:
T ~ 0.5 x 104 K
xe ~ 10-2; Cosmic Rays

CNM:
T ~ 50 K
xe ~ 10-4; Carbon+

The “bottom part” of the superbubble. Top panel is WIM (Halpha); Bottom Panel is WNM/CNM (21-cm). NOTE THE THREE RECTANGLES!

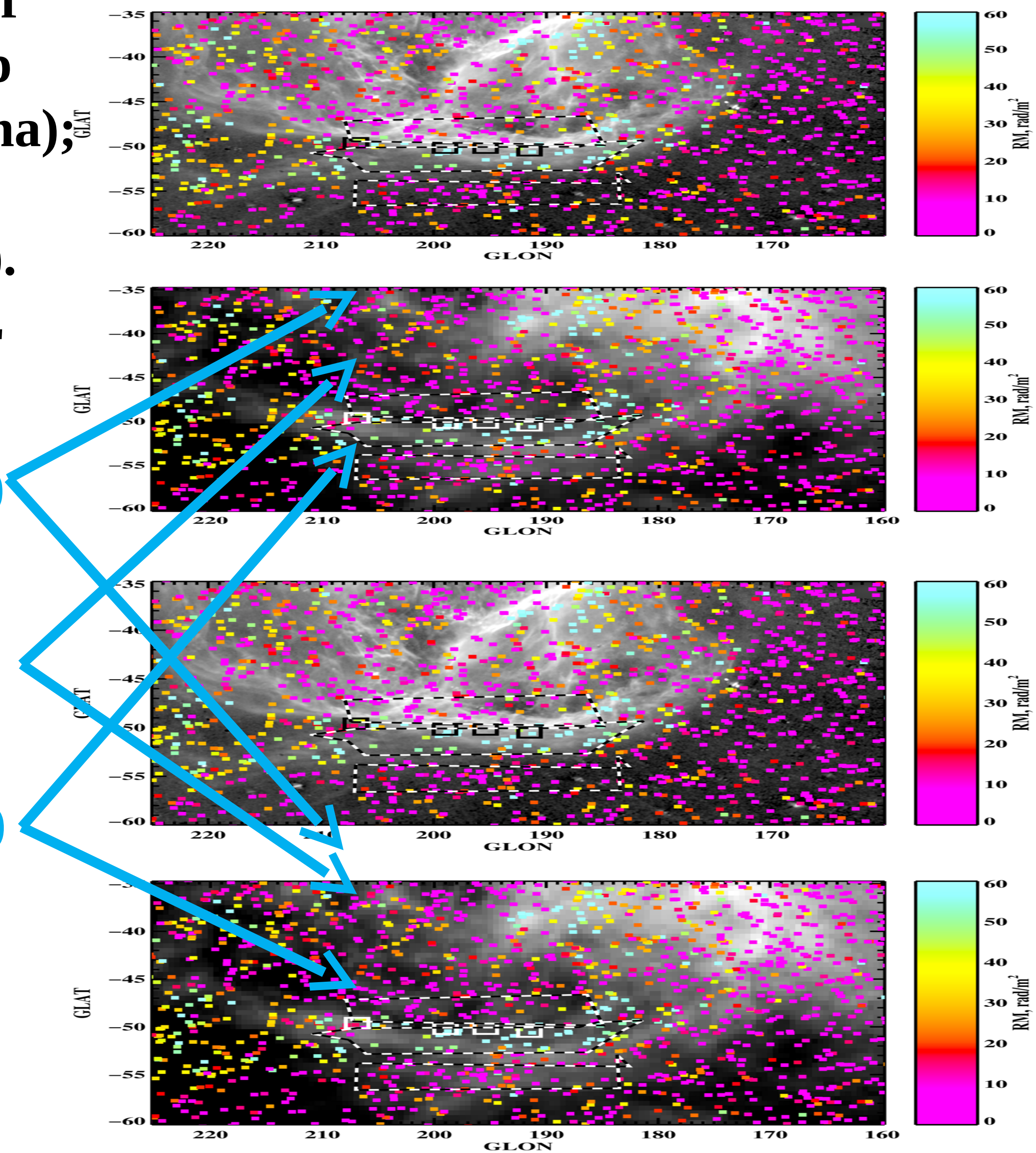

Inside (IN)

(EDGE)

Outside (OUT)

Let’s do some numbers…

We see Δ(RM) ~ 60 rad m-2

Δ(EM)20 ~ 1.4; (B||/ne~1.7 µG-cm3)

If PWIM~4000 cm-3 K, then ne~0.25 cm-3 and

L~740 pc, B||~0.4 µG

¡¡TOTALLY UNREASONABLE!!

Much more reasonable:

B|| = 10 μG (same as from HI Zeeman splitting in the vicinity)

ne ~5.9 cm -3

L~30 pc

PWIM~94000 cm-3-K

Btot = 20 μG, Pmag= 100000 cm-3-K

P seems large, but it is comparable to hot gas pressure inside the bubble.

EM Histograms

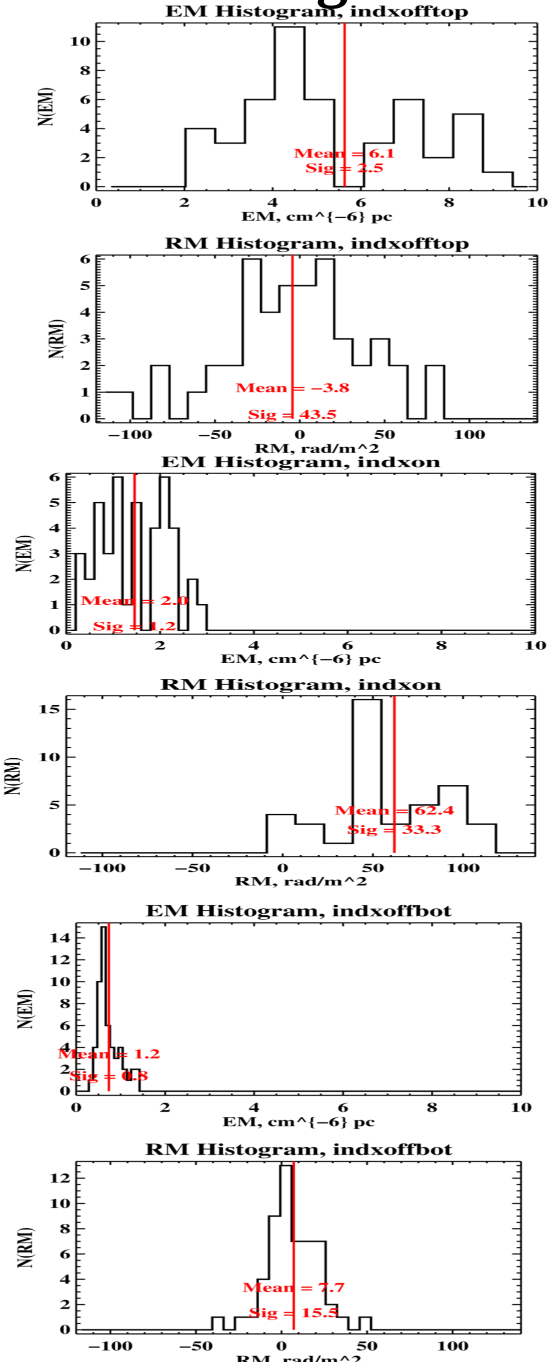

(IN)

(EDGE)

(OUT)

RM Histograms

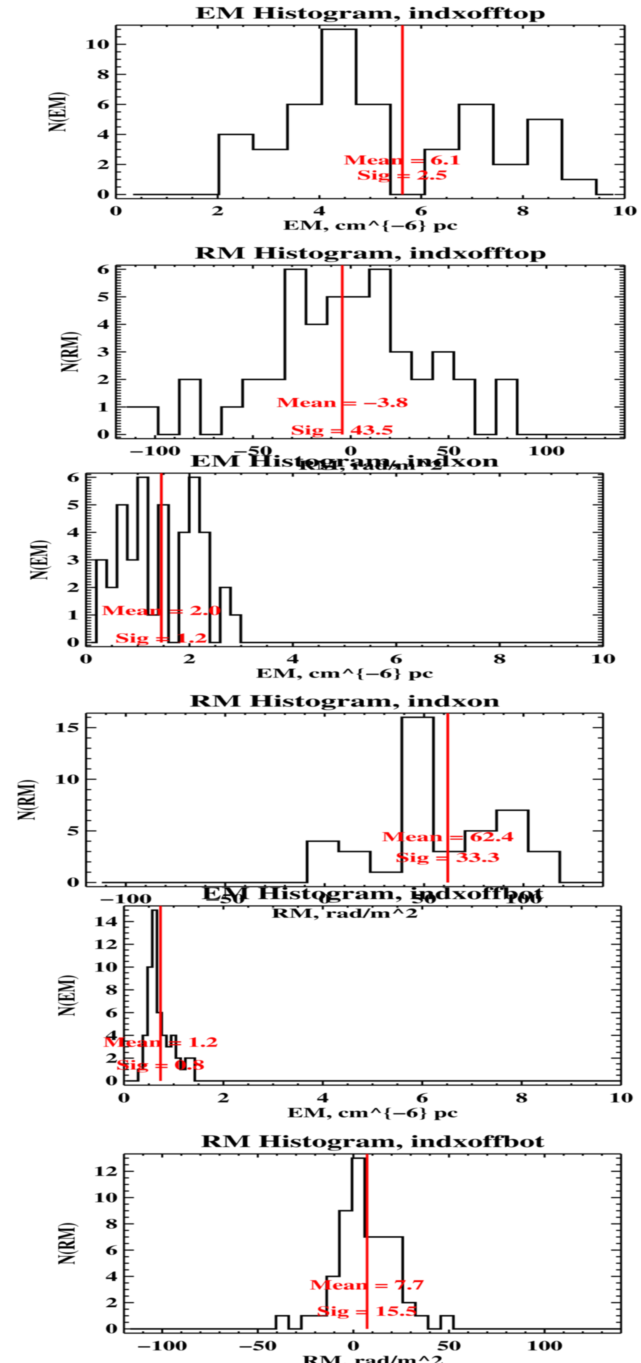

Consider a superbubble that has swept up the internal field into its shell.

The upper panel shows a field line.

The lower panel shows the Faraday Rotation Measure RM of this swept-up field.

The observer looks UP from BELOW.

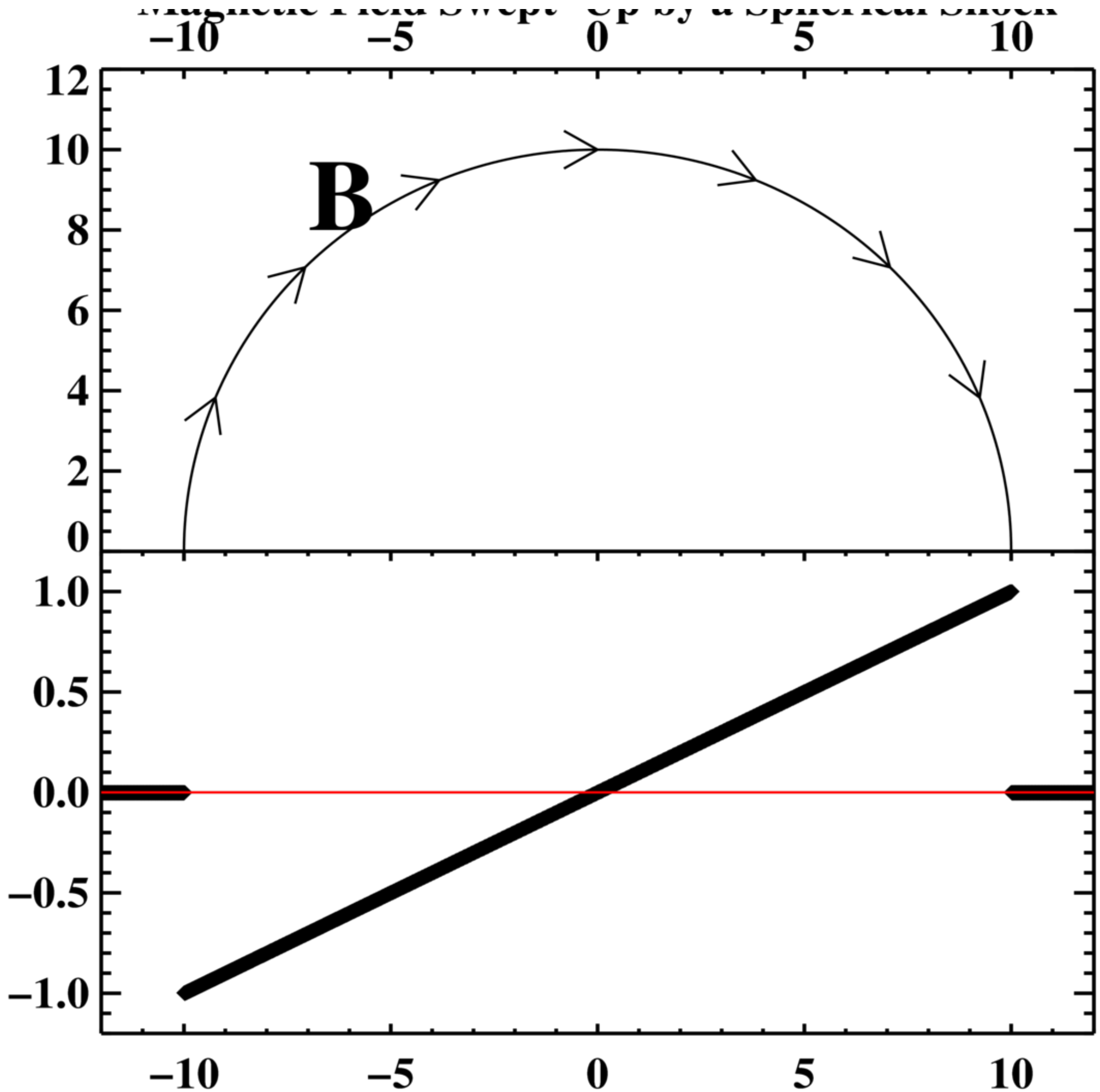

Now for a corrugated field line.
The upper panel shows the corrugated field line.
The lower panel shows its RM.

Again, the observer looks UP from BELOW.

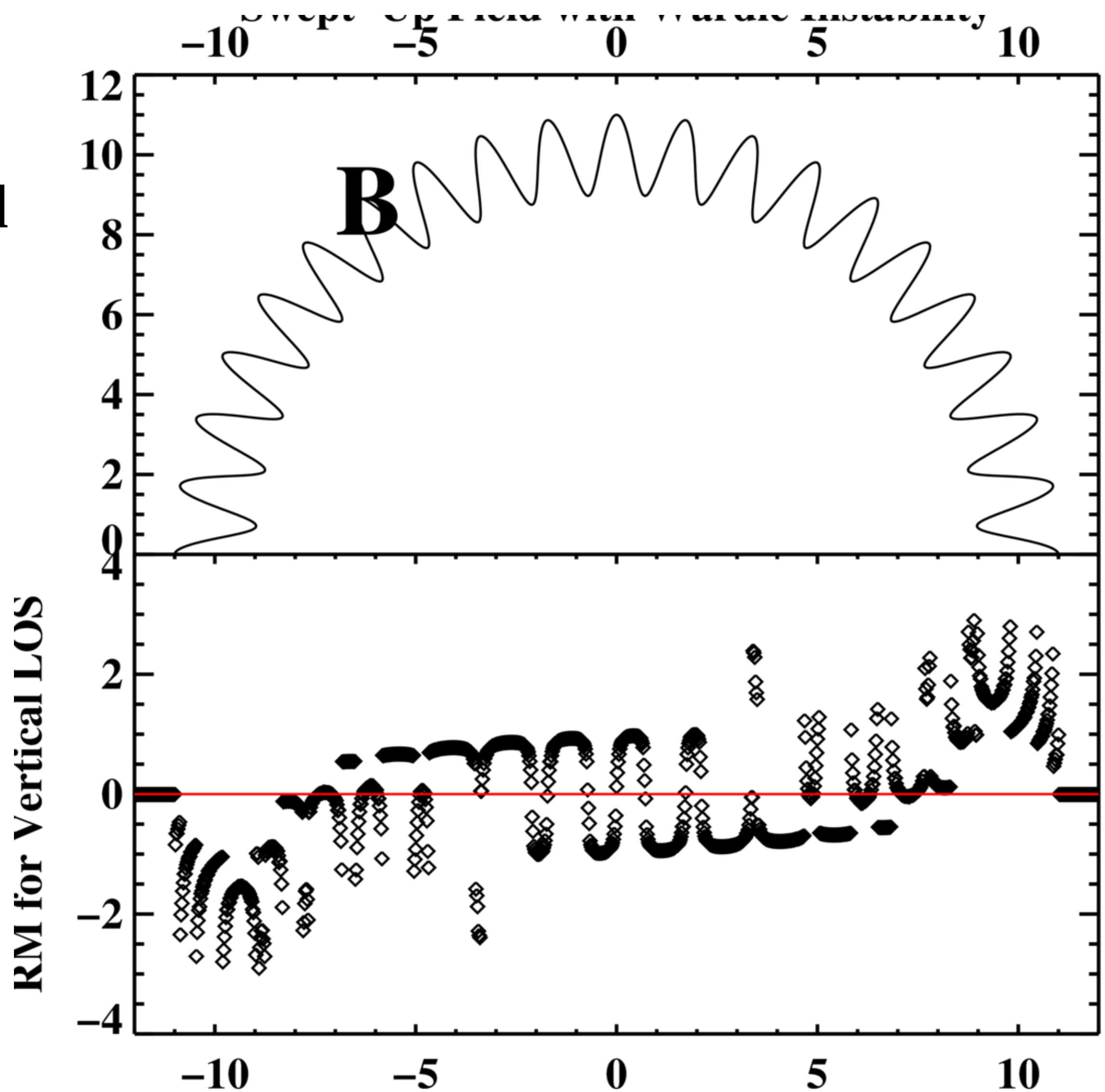

Is the corrugation from the Wardle instability?

From Draine & McKee 1993, ARA&A Review

Now consider what would happen if the straight magnetic field lines of the plane-parallel steady solution were to be perturbed as in Figure 4. The drag force will now have a component parallel to the local magnetic field that cannot be balanced by the $\mathbf{J} \times \mathbf{B}$ force, and ions will therefore be accelerated along the field lines to collect in the magnetic "valleys." As a consequence, $\rho^{(i)}$ will increase in the valleys, the drag force (proportional to $\rho^{(i)}$) will increase, and the field lines may be further distorted. Linear stability analysis (Wardle 1990) found C-type MHD shocks with $B_{\|} = 0$ to be unstable for $M_A \gtrsim 5$; oblique shocks (in which $B_{\|} \neq 0$) behave similarly (Wardle 1991b). The nonlinear development has yet to be investigated, so that it is not yet known to what degree these unstable shocks will differ from the idealized steady-flow solutions that have been studied numerically. The most unstable mode has a wavelength approximately equal to the thickness of the shock transition.

5.3 *Cosmic-Ray-Mediated Shocks: Drury Instability*

Shocks which are efficient at cosmic-ray acceleration have a postshock cosmic-ray pressure that is an appreciable fraction of the total momentum flux $\rho_0 v_s^2$. As a result, the cosmic-ray pressure gradient in the neighborhood of the shock is dynamically significant. Drury (1984) noted that acoustic

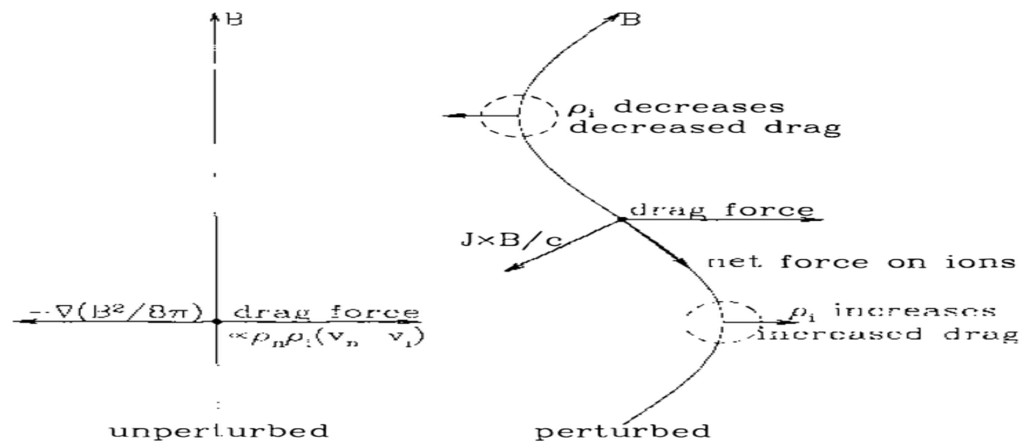

Figure 4 Mechanism for the Wardle instability in two-fluid MHD shock waves.

EM Structure F’cn

RM Structure F’cn

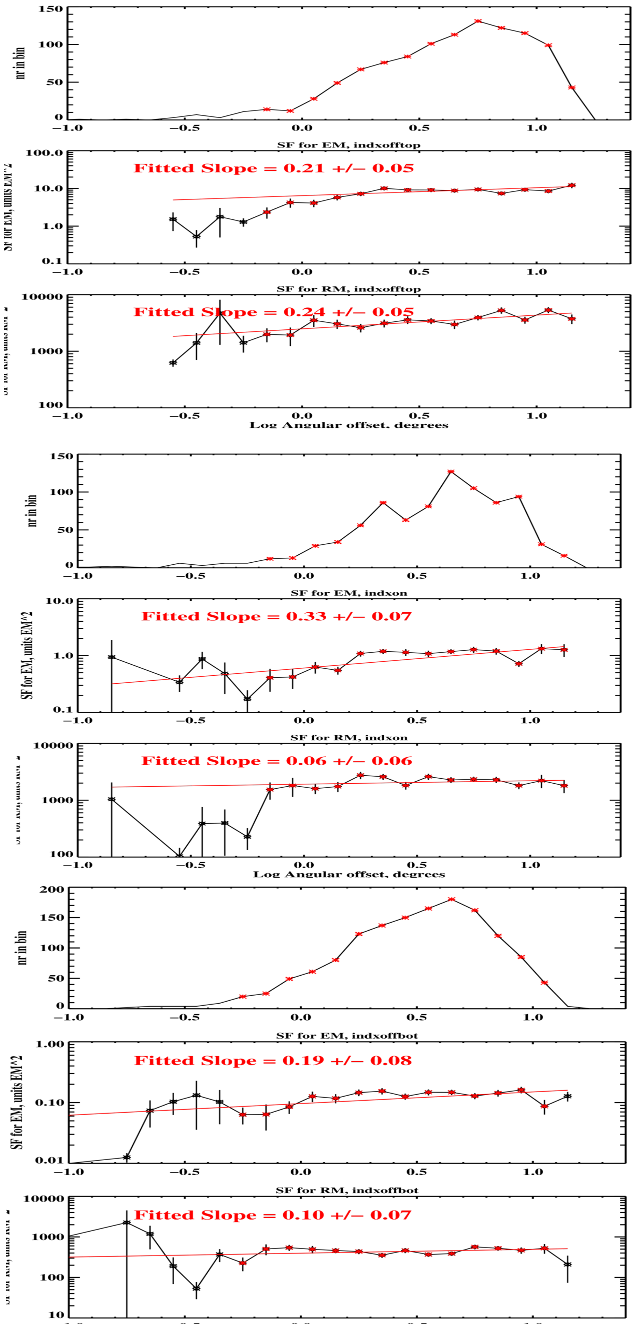

(IN)

(EDGE)

(OUT)

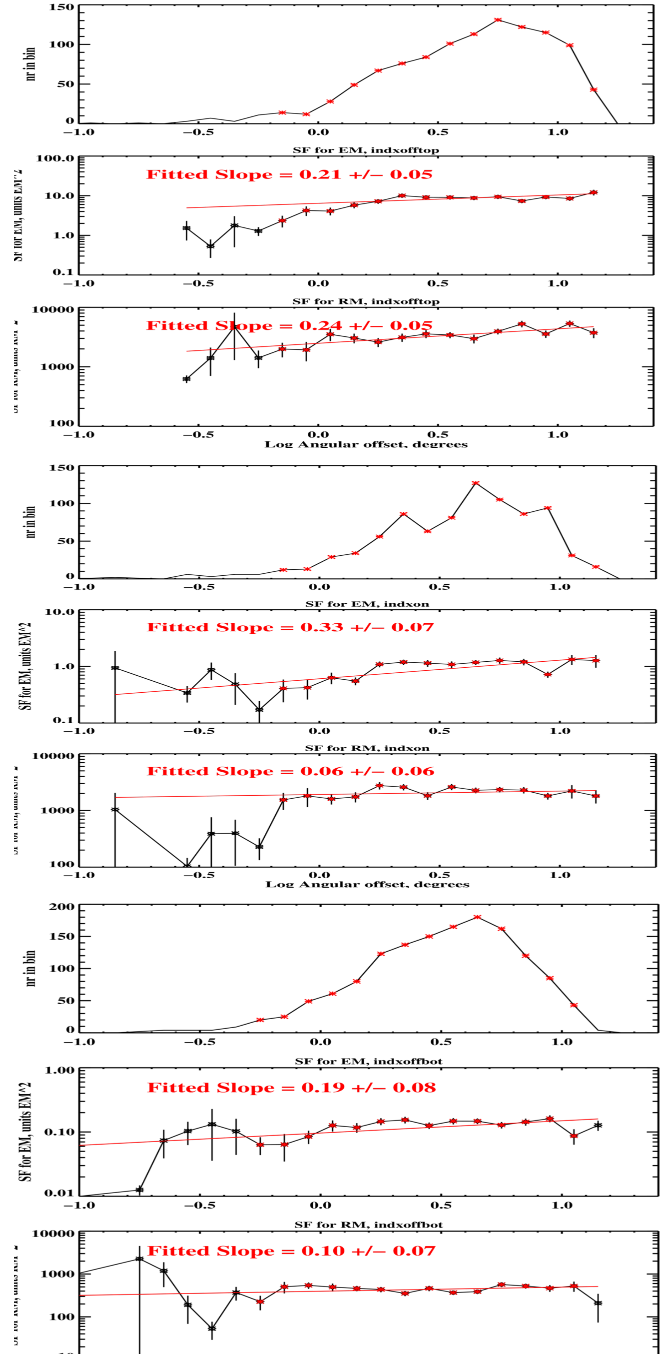

For Kolmogoroff turbulence, the structure functions would have a logarithmic slope of 5/3. For 2-d turbulence, the slope would be 2/3 (Minter & Spangler 1998).

But the slopes are essentially FLAT.

This means that the fluctuation scale—the outer scale for turbulence—is SMALLER THAN OUR EFFECTIVE RESOLUTION, which is about 0.6 degrees, or a few parsec.

THE FLUCTUATION SCALE IS LESS THAN A FEW PC.

Current Summary:

We see that Superbubble walls are interesting:

-They sometimes are magnetically dominated (probably usually!)

-They should have WPIM (if there is HIM nearby, like inside the very same superbubble)

-They sometimes have huge RMs

-They sometimes have corrugated field lines

-The scale length of the corrugations is surprisingly (to me) small

Let’s turn to a larger philosophical issue:

People fit off-plane RMs to derive the global magnetic field configuration in the 'Galactic Halo':

--Vertical 'Halo' field near Sun: Taylor et al. and Mao et al. agree for SGP (RM= [-6.7 +/- 0.5] rad/m2), disagree for NGP ([3.1 +/- 0.5] vs [0.0 +/- 0.5] rad/m2).

--Horizontal 'Halo' field near Sun: Taylor et al. find -0.4 μG at b= +45, +0.8 μG at b= -45, towards l~280. NOTE: they find a REVERSAL above/below b=0!

This reversal agrees with Han et al. A picture:

The Galactic Halo according to Han (2009). Antisymmetric RMs: the signs reverse across the b=0 line and across the l=0 line. This leads to the global field configuration on the right hand side, which is consistent with an A0 dynamo.

462 J. L. Han

region. However, this is the volume-averaged field strength in such a large region. The poloidal fields are possibly limited to a smaller central region. The newly discovered "double helix" nebula (Morris et al. 2006), with an estimated field strength of order 100 μG, reinforces the presence of strong poloidal magnetic fields in tube format merging from the rotating circumnuclear gas disk near the Galactic Center.

Polarized thermal dust emission has been detected in the molecular cloud zone at sub-mm wavelength (see Fig. 4, Novak et al. 2003, Chuss et al. 2003), which is probably related to the toroidal fields parallel to the Galactic plane and complements the poloidal fields shown by the vertical filaments. The observed molecular cloud zone has a size of a few hundred pc, and is possibly a ring-like cloud outside the central region with poloidal field (see Fig.1 of Chandran 2001). The sub-mm polarization observations of the cloud zone offer information only about the field orientations. Zeeman splitting measurements of HI absorption against Sgr A (e.g. Plante et al. 1995) or of the OH maser in the Sgr A region (Yusef-Zadeh et al. 1999) give a line-of-sight field strength of a few mG in the clouds. It is possible that toroidal fields in the clouds are sheared from the poloidal fields, so that the RM distribution of radio sources in this very central region could be antisymmetric (Novak et al. 2003).

Outside the central region of a few hundred pc to a few kpc, the structure in the stellar and gas distributions and the magnetic structure are all mysterious. There probably is a bar. The large-scale magnetic fields should be closely related to the material structure but have not been revealed yet. The large positive RMs of background radio sources within $|l| < 6°$ of the Galactic Center (Roy et al. 2005) are probably related to magnetic fields following the bar (Roy et al. 2008). Comparison of the RMs of these background radio sources with RMs of foreground pulsars (see Fig. 1) should be helpful in delineating the field structure.

4. Magnetic fields in the Galactic halo

Magnetic field structure in the Galactic halo can be revealed from RMs of EGRs if allowance can be made for sources with outstanding intrinsic RMs. The foreground Galactic RM is the common contribution to the observed RMs of all EGRs within a small patch of sky. After "anomalous" RMs are eliminated, the pattern for the Galactic RM can be obtained. Han et al. (1997) discarded any source if its RM deviated from the average RM of neighbouring sources by more than 3σ, and obtained a "cleaned" RM sky.

A striking antisymmetry in the inner Galaxy with respect to Galactic coordinates (see

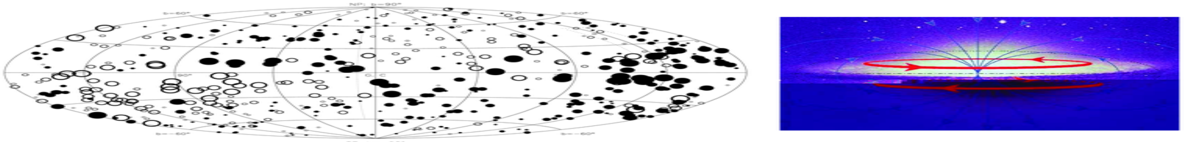

Figure 5. The antisymmetric rotation measure sky, derived from RMs of extragalactic radio sources after filtering out the outliers with anomalous RM values. The distribution corresponds to magnetic structure in the Galactic halo as illustrated on the right. See Han et al. (1997, 1999).

These 'halo field models' use high-latitude RMs, so they rely on the field within ~1 kpc reliably tracing the Galactic-wide halo field. The huge RM fluctuations at high latitudes produced by identifiable, individual ISM structures produce `cosmic variance' and I suspect this is serious.

Our high-latitude RM data sample about 1/64 of the Galactic plane's area. Do you believe it's reliable to extrapolate this tiny area to the whole Galaxy?
What would we measure if we moved 1 kpc away from our present position?

SUMMARY

We see that Superbubble walls are interesting:

-They sometimes are magnetically dominated (probably usually!)
-They should have WPIM (if there is HIM nearby, like inside the very same superbubble)
-They sometimes have huge RMs
-They sometimes have corrugated field lines
-The scale length of the corrugations is surprisingly (to me) small

and…

The high-latitude sky's RMs are dominated by individual structures. In my opinion, we should be cautious about using high-latitude RMs to make statements about the Global Galactic Field.

Fin

We (or at least I; how about you?) believe that high-latitude RMs are dominated by INDIVIDUAL STRUCTURES—contrary to conventional viewpoint that they trace the GLOBAL GALACTIC FIELD.

THE ASTROPHYSICAL JOURNAL, 702:1230–1236, 2009 September 10

doi:10.1088/0004-637X/702/2/1230

A ROTATION MEASURE IMAGE OF THE SKY

A. R. TAYLOR, J. M. STIL, AND C. SUNSTRUM
Department of Physics and Astronomy, and Institute for Space Imaging Science, University of Calgary, AB, Canada
Received 2009 March 28; accepted 2009 July 20; published 2009 August 19

ABSTRACT

We have re-analyzed the NRAO VLA Sky Survey (NVSS) data to derive rotation measures (RMs) toward 37,543 polarized radio sources. The resulting catalog of RM values covers the sky area north of declination $-40°$ with an average density of more than one RM per square degree. We present an image of the median RM over 82% of the sky with a resolution of 8° and a typical error of ± 1–2 rad m^{-2}. The image shows large-scale structures in RM that extend to very high Galactic latitudes. A simple analysis of the RM structure at high Galactic latitudes is used to derive properties of the Galactic halo magnetic field in the solar neighborhood. We find the component of the local field perpendicular to the plane (the z-component) equal to +0.30 μG for $z < 0$ and -0.14 μG for $z > 0$. The reversal of sign across the Galactic plane is consistent with a quadrupole field geometry for the poloidal component of the halo field. The halo magnetic field component parallel to the disk is also found to be antisymmetric and generally consistent with a toroidal field, with strength +0.83 μG for $z < 0$ and -0.39 μG for $z > 0$. We have identified five regions of the sky where the foreground median RM is consistently less than 1 rad m^{-2} over several degrees. These holes in the foreground RM will be useful for future studies of possible small-scale fluctuations in cosmic magnetic field structures. In addition to allowing measurement of RMs toward polarized sources, the new analysis of the NVSS data removes the effects of bandwidth depolarization for $|\mathrm{RM}| \gtrsim 100$ rad m^{-2} inherent in the original NVSS source catalog. This new catalog of RMs and polarized flux densities is available online, and will be a valuable resource for further studies of the Galactic magnetic field and magnetoionic medium, and extragalactic magnetic fields.

Key words: catalogs – Galaxy: halo – magnetic fields – polarization

1. INTRODUCTION

Faraday rotation of the polarized synchrotron radiation from radio sources provides a probe of the magnetic field and thermal electron density along the line of sight. Observations of Faraday rotation measures (RMs) have been carried out since the 1960s through measurements of the wavelength dependence of polarization position angles at widely separated frequencies (e.g., Gardner & Whiteoak 1963). Compilations of published RMs were created for 555 objects by Simard-Normandin et al. (1981) and 674 objects by Broten et al. (1988). More recently, spectropolarimetric surveys of the Galactic plane (Taylor et al. 2003; Haverkorn et al. 2006) have added 528 published RM values at low Galactic latitudes (Brown et al. 2003a, 2007), while Gaensler et al. (2005) and Mao et al. (2008) have measured ~300 RMs in the vicinity of the LMC and SMC.

The low-latitude data have been used to explore the Galactic magnetic field (Brown et al. 2003b, 2007) and the magnetoionic component of the interstellar medium (Haverkorn et al. 2008). However, the low surface density of RM at higher latitudes has precluded the use of extragalactic RMs for conclusive studies of the Galactic halo field. Xu et al. (2006) used an augmented version of the Simard-Normandin et al. (1981) catalog, containing approximately 1000 high-latitude RM values, to search for evidence of enhanced RM associated with nearby galaxy superclusters. They report tentative detections against the Hercules and Perseus-Pisces clusters, but note that "conclusions must remain tentative until we better understand the Galactic foreground."

The most extensive large-area survey of polarized radio sources to date is the National Radio Astronomy Observatory VLA Sky Survey (NVSS) which observed the sky north of declination $-40°$ (82% of the sky) in Stokes I, Q, and U at a frequency of 1.4 GHz (Condon et al. 1998). The NVSS images and source catalog were created by combining 217,446 VLA snapshot observations in two bands, each 42 MHz wide, at 1364.9 MHz and 1435.1 MHz. Faraday rotation will produce a rotation of the polarization angle between the two bands. The effects of bandwidth depolarization on the number density of polarized sources in the NVSS catalog due to integrating over the two bands in regions of high foreground RM was reported by Stil & Taylor (2007). We have reprocessed the NVSS visibility data to create images in each of the two bands, and analyzed the data to calculate RMs for compact polarized sources. In this paper, we present the catalog of 37,543 polarized sources with RMs and polarized intensities corrected for the depolarization in the original values from the NVSS catalog. We also carry out a simple analysis on the data to derive some basic properties of the Galactic halo magnetic field.

2. THE DATA

2.1. Derivation of Rotation Measures

To derive RM values from the NVSS observations, we downloaded the calibrated NVSS visibility data sets for each snap shot from the National Radio Astronomy Observatory data server and created mosaic images in Stokes I, Q, and U in each of the two bands. The images were created using AIPS. A mosaic weight image was also created to provide an estimate of the theoretical noise as a function of position. We also created images with combined data from both bands to measure the amount of depolarization. Since we use the peak intensity as an estimate of the source flux, a mild u–v taper was applied, degrading the resolution slightly compared to the original NVSS images to mitigate resolution effects. The peak flux density was measured in each image at the position of every NVSS catalog source with cataloged Stokes I intensity greater than 5 mJy. The noise level, σ, for the Q and U values was determined

People fit RMs to Galactic global field models. In the Galactic plane:

Han et al., van Eps et al., Haverkorn et al. find that field lines follow spiral arms with pitch angle decreasing with Galactocentric radius, with reversals. Details differ.

Some pictures:

The Galaxy according to Han (2009). Arm/interarm reversals of field lines that follow spiral arms.

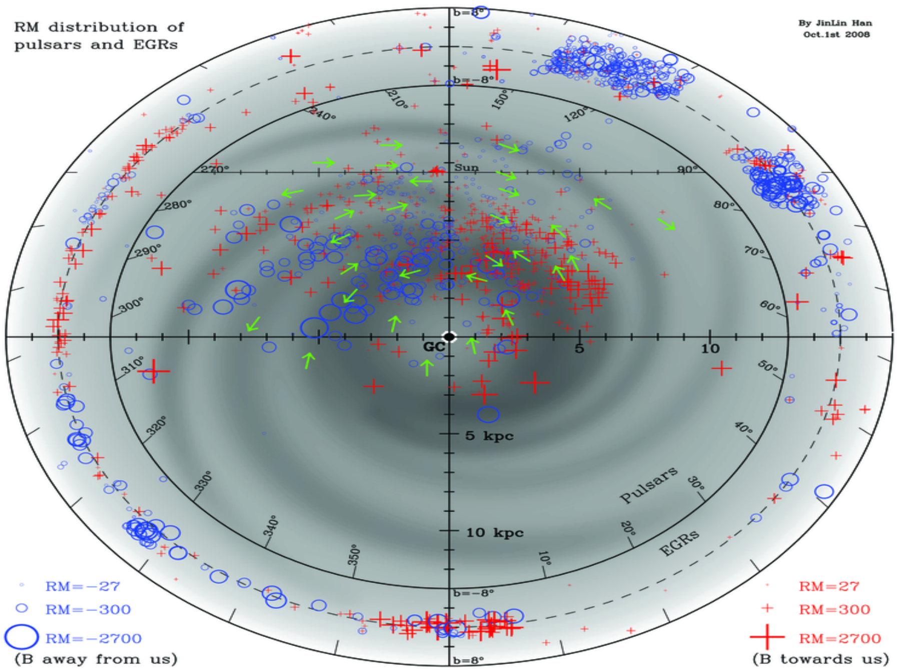

Figure 1. The RM distribution of 736 pulsars with $|b| < 8°$ projected onto the Galactic plane, including new data of Han et al (2009, in preparation). The linear sizes of the symbols are proportional to the square root of the RM values with limits of ± 27 and ± 2700 rad m^{-2}. Positive RMs are shown by plus signs and negative RMs by open circles. The background shows the approximate locations of spiral arms used in the NE2001 electron density model (Cordes & Lazio 2002). RMs of 1285 EGRs of $|b| < 8°$ (data mainly from Clegg et al. 1992, Gaensler et al. 2001, Brown et al. 2003, Roy et al. 2005, Brown et al. 2007 and other RM catalogs) are displayed in the outskirt ring according to their l and b, with the same convention of RM symbols and limits. The large-scale structure of magnetic fields indicated by arrows was derived from pulsar RMs and comparison of them with RMs of background EGRs (details in Han et al. 2009). The averaged RM fluctuations with Galactic longitudes of EGRs are consistent with magnetic field directions derived from pulsar data, for example, in the 4th Galactic quadrant.

terstellar medium mostly in tangential regions. The fluctuations in the RM distribution of extragalactic radio sources (Clegg et al. 1992, Gaensler et al. 2001, Brown et al. 2003, Roy et al. 2005, Brown et al. 2007) with Galactic longitude, especially these of the fourth Galactic quadrant, are consistent with magnetic field directions derived from pulsar data (see Fig. 1). The negative RMs of EGRs in the 2nd quadrant suggest that the interarm fields both between the Sagittarius and Perseus arms and beyond the Perseus arm are predominantly clockwise.

The Galaxy according to Van Eck et al. (2011): One spiral-shaped reversal, only inside the Solar circle.

Field Strength

Field Morphology

MODELING THE MAGNETIC FIELD IN THE GALACTIC DISK 11

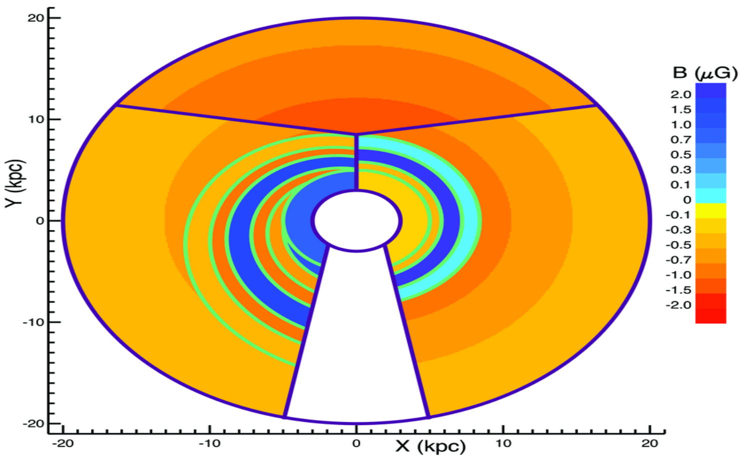

FIG. 10.— Best-fit magnetic field strengths for each of the regions shown in the lower panel of Figure 6. Shades of orange/red represent clockwise field, while shades of blue represent a counter-clockwise field.

VAN ECK ET AL.

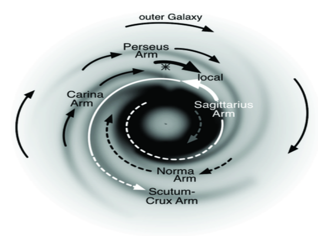

11.— A sketch of the magnetic field in the disk of the Galaxy based on ork. The bold arrows in the local arm and Q1 of the Sagittarius-Carina ows the only generally accepted location of the large-scale reversal in e discussion in Brown 2011). The remaining arrows show the field ons as concluded from this study. The dashed arrows are less certain the paucity of data available in these regions.

5. SUMMARY AND DISCUSSION

have processed a set of VLA observations and produced alog of 194 rotation measures of extragalactic sources Galactic disk, filling in critical gaps in rotation mea- coverage between the Canadian Galactic Plane Survey e Southern Galactic Plane Survey. Using these data, we ude that of the three popular models investigated by Sun (2008), the most consistent with our new data is the -RING model.

propose our own model, stemming from a new model- rategy that studies the disk field in three different sectors. livision of sectors is roughly between the outer Galaxy rants 2 and 3), quadrant 1 and quadrant 4. Our modeling sts that the inner Galaxy has a spiral magnetic field that ned with the spiral arms, while the outer Galaxy is dom- l by an almost purely azimuthal field. This is consistent a significant decrease of the magnetic pitch angle with alactocentric radius, to small (almost zero) values be- the Solar orbit. Such a decrease is also seen in external galaxies (Fig. 8 in Beck et al. 1996). For example, the angle in M31 decreases from $-19\pm3°$ near the galactic r to $-8\pm3°$ at $r = 12$–14 kpc (Fletcher et al. 2004).

r model also indicates that the magnetic field in the y is predominantly clockwise, with a single reversed re- hat appears to spiral out from the center of the Galaxy. is similar to the ASS+ARM model described by Sun et 2008), except that the pitch angle varies with radius in odel. In some sense, our model provides a 'unification' two axisymmetric spiral models discussed by Sun et al. 8).

origin of magnetic reversals remains poorly under- . An obvious possibility to explain them is a bisymmet- agnetic field (perhaps of primordial origin; see Sofue 1986, and references therein). A bisymmetric mag- structure has reversals between spiral-shaped regions, oth in radius and azimuth. However, it is now believed isymmetric magnetic fields are rare in spiral galaxies, and that galactic magnetic fields are maintained by some form of dynamo action (Beck et al. 1996). Dynamo mechanisms generally favor axisymmetric magnetic structures, with non-axisymmetric features resulting from secondary effects (such as the spiral pattern and/or overall galactic asymmetry). Our results indicate that the regular magnetic field in the outer part of the Milky Way is predominantly axisymmetric. Ruzmaikin et al. (1985) suggested that radial reversals of an axisymmetric magnetic field can be maintained, for periods comparable to the galactic lifetime, provided the initial (seed) magnetic field had such reversals, for example if the seed field was random (resulting, e.g., from the fluctuation dynamo action). Ruzmaikin et al. (1985) confirmed that a few reversals can persist in the Milky Way if the half-thickness of the ionized layer is within the range 350–1500 pc, whereas this range is much narrower in the case of M31, 350–450 pc (these estimates can be model-dependent). This seems to explain the presence of at least one reversal in the Milky Way and their absence in M31. Asymptotic analysis of the mean-field galactic dynamo equations with α-quenching (Belyanin et al. 1994) shows that the radial reversals can be persistent at those galactocentric radii r where

$$r^2\gamma(r)\left(\frac{1}{r}+2\frac{B_0'(r)}{B_0(r)}\right)+\frac{1}{2}r^2\gamma'(r)=0,$$

where $\gamma(r)$ is the local growth rate of the regular magnetic field due to the dynamo action, $B_0(r)$ is its local saturation strength (presumably corresponding to the energy equipartition with the turbulent energy), and prime denotes derivative with respect to radius (see Shukurov 2005, for a review). Thus, the occurrence of the reversals is sensitive to rather subtle details of the galactic dynamo that are poorly known. This severely restricts the predictive power of the theory and limits the value of numerical results, which are inevitably obtained with idealized and often heavily parameterized models.

As another way to visually examine our modeling efforts, we have combined our 3 magnetic sectors with NE2001 to produce a rotation measure map at $z = 0$, as shown in Figure 12. The small circles along the interior show the pulsar RMs, and the larger circles around the outside (at $R = 20$ kpc) are the smoothed (9° bin widths, 3° steps between bins) EGS RMs, corresponding to the middle plot in Figures 7 through 9. While certainly there are places where the data and the model disagree in Figure 12 (likely due to small scale fluctuations in the data that have not been accounted for and perhaps also due to the limitations of the model), overall the data appears to be fitted quite well. Were it not for the black circles on the data points, many of these points would be virtually indistinguishable from the background model.

We expect that significant improvements on this model, using the same technique and the present edition of the electron density model, will be difficult to accomplish for several reasons. First, the electron density model includes very little small scale structure beyond the local regions. Second, the reliability of distances to the pulsars remains questionable; small shifts in the assumed position of the pulsars will influence the results of the best fit. Fortunately, the EGS are simply assumed to be located at the edge of the Galaxy in their identified ℓ, b direction, making their 'position' reliable. Therefore, they can provide a stable base to assess the model. Finally, as is always the case with modeling, more data would vastly improve the model. For example, pulsars on the far side of the Galactic center would provide much needed constraints

The in-plane models are getting really good at matching the RM data! The data sample large swaths of the Galactic plane. Even though current studies differ on the details, I believe that IN PRINCIPLE the approach is valid and, with lots more data, will reveal the truth.

Fin

Fin

The original four phases, as defined by McKee & Ostriker, are not the four we think of today.

Today it's:

***The essentially <u>FULLY NEUTRAL</u> CNM and WNM**

***The essentially <u>FULLY IONIZED</u> WIM and HIM**